ERR agonism reverses mitochondrial dysfunction and inflammation in the aging kidney

Xiaoxin X. Wang[1], Komuraiah Myakala[1], Andrew E. Libby[1], Suman Ranjit[1], Shogo Takahashi[1], Bryce A. Jones[2], Kanchan Bhasin[1], Yue Qi[3], Kristopher W. Krausz[4], Patricia M. Zerfas[5], Julia Panov[6,7], Thomas J. Velenosi[4], Daxesh P. Patel[4], Parnaz Daneshpajouhnejad[8], Avi Titievsky[6], Vadim Sharov[6], Boris Ostretsov[6], Cyrielle Billon[9], Arindam Chatterjee[10], John K. Walker[10], Jeffrey B. Kopp[11], Avi Z. Rosenberg[8], Frank J. Gonzalez[4], Udayan Guha[3], Leonid Brodsky[6], Thomas P. Burris[9], Moshe Levi[1]

[1]Department of Biochemistry and Molecular & Cellular Biology, [2]Department of Pharmacology and Physiology, Georgetown University, Washington DC 20057, USA; [3]Thoracic and GI Malignancies Branch, National Cancer Institute, National Institutes of Health, Bethesda, MD 20814, USA; [4]Laboratory of Metabolism, Center for Cancer Research, National Cancer Institute, National Institutes of Health, Bethesda, MD 20892, USA; [5]Office of Research Services, Office of the Director, National Institutes of Health, Bethesda, MD 20892, USA; [6]Tauber Bioinformatics Research Center, [7]Sagol Department of Neurobiology, University of Haifa, Mount Carmel, Haifa, 31905, Israel; [8]Department of Pathology, Johns Hopkins University School of Medicine, Renal Pathology Service, Baltimore, MD 21287, USA; [9]Center for Clinical Pharmacology, Washington University School of Medicine and St. Louis College of Pharmacy, St. Louis, MO 63110, USA; [10]Department of Pharmacology & Physiology, Saint Louis University School of Medicine, St. Louis, MO 63104, USA; [11]Kidney Diseases Branch, National Institute of Diabetes and Digestive and Kidney Diseases, National Institutes of Health, Bethesda, MD 20814, USA

Correspondence:

Moshe Levi
Department of Biochemistry and Molecular & Cellular Biology,
Georgetown University,
3900 Reservoir Road, Basic Science 353,
Washington DC 20057, USA
Tel: 202-687-9296
E-mail: Moshe.Levi@georgetown.edu

ABSTRACT (147 words)

A gradual decline in renal function occurs even in healthy aging individuals. In addition to aging per se, concurrent metabolic syndrome and hypertension, which are common in the aging population, can induce mitochondrial dysfunction, and inflammation, which collectively contribute to age-related kidney disease. Here we studied the role of the nuclear hormone receptors, the estrogen related receptors (ERRs) in regulation of age-related mitochondrial dysfunction and inflammation. ERRs are decreased in aging human and mouse kidneys and preserved in aging mice with lifelong caloric restriction (CR). Our studies identified ERRs as important modulators of age-related mitochondrial dysfunction and inflammation. ERRα, ERRβ, and ERRγ levels are decreased in the aging kidney. Remarkably, only a 4-week treatment of 21-month-old mice with the pan ERR agonist reversed the age-related increases in albuminuria and podocyte loss, mitochondrial dysfunction and inflammatory cytokines, including the cGAS-STING and STAT3 signaling pathways. A 3-week treatment of 21-month-old mice with a STING inhibitor reversed the increases in inflammatory cytokines and the senescence marker p21 but also unexpectedly reversed the age-related decreases in PGC-1α, ERRα, mitochondrial complexes and Mcad expression.

INTRODUCTION

The fastest growing US population with impaired kidney function is the 65 and older age group. This population is expected to double in the next 20 years, while the number worldwide is expected to triple from 743 million in 2009 to 2 billion in 2050. This will result in a marked increase in the elderly population with chronic kidney disease and acute kidney injury. This increase may be further amplified by other age-related co-morbidities including metabolic syndrome and hypertension that accelerate age-related decline in renal function [1]. Thus, there is an increasing need for prevention and treatment strategies for age-related kidney disease.

A gradual age-related decline in renal function occurs even in healthy aging individuals [2]. Progressive glomerular, vascular and tubulointerstitial sclerosis is evident on renal tissue examination of healthy kidney donors with increasing age [3]. In addition to aging *per se*, metabolic syndrome and hypertension can induce mitochondrial dysfunction and inflammation, as well as endoplasmic reticulum stress, oxidative stress, altered lipid metabolism, and elaboration of profibrotic growth factors in the kidney, which collectively contribute to age-related kidney disease [2].

There is variation in the rate of decline in renal function as a function of sex, race, and burden of co-morbidities [4-6]. Interestingly, examination of processes leading to sclerosis suggests a role for possible modifiable systemic metabolic and hormonal factors that can ameliorate the rate of sclerosis. With the population of older individuals increasing, identifying preventable or treatable aspects of age-related nephropathy becomes of critical importance.

There is increasing evidence that mitochondrial biogenesis, mitochondrial function, mitochondrial unfolded protein response (UPR^{mt}), mitochondrial dynamics, and mitophagy are impaired in aging, and these alterations contribute to the pathogenesis several of the age-related diseases [7-9]. In this regard current studies are concentrated on modulating these molecular mechanisms to improve mitochondrial function.

Caloric restriction (CR) plays a prominent role in preventing age-related complications. We have previously shown that CR prevents the age-related decline in renal function and renal lipid accumulation via, at least in part, inhibition of the function of sterol regulatory element binding proteins (SREBPs) [10, 11]. CR is also an important modulator of mitochondrial function. We have demonstrated that CR prevents age-related mitochondrial dysfunction in the kidney by increasing the following: mitochondrial/nuclear DNA ratio, mitochondrial complex activity including fatty acid β-oxidation and expression of the mitochondrial transcription factor NRF1, the protein kinase AMPK, the deacetylases sirtuin 1 and 3, and mitochondrial isocitrate dehydrogenase (IDH2) expression [12]. In addition, CR also prevents the age-related decrease in mitochondrial number in the renal tubules. CR increases expression of the bile acid regulated nuclear receptor farnesoid X receptor (FXR) and the Takeda G protein coupled receptor (TGR5). Treatment of 22-month-old *ad lib* (AL)-fed mice for 2 months with the dual FXR-TGR5 agonist INT-767 reversed most of the age-related impairments in mitochondrial function and the progression of renal disease [12]. Importantly INT-767 and CR each increased expression of PGC-1α, ERRα, and ERRγ, which are important regulators of mitochondrial biogenesis and function.

The estrogen-related receptors (ERRs) ERRα (NR3B1, ESSRA gene), ERRβ (NR3B2, ESRRB gene), and ERRγ (NR3B3, ESRRG gene) are members of the nuclear receptor superfamily. While one report suggests a role for cholesterol [13], there are no confirmed endogenous ligands for these orphan receptors. Importantly the ERRs do not bind natural estrogens, and they do not directly participate in classic estrogen signaling pathways or biological processes [14]. ERRα and ERRγ are strongly activated by their coactivators PGC-1α and PGC-1β [15]. In contrast, RIP140 and NCoR1 are important corepressors of ERR activity [16, 17]. ERRs are subject to post-translational modifications including phosphorylation, sumoylation, and acetylation that modulate their DNA binding and recruitment of coactivators [18, 19].

ERRα and ERRγ regulate the transcription of genes involved in mitochondrial biogenesis, oxidative phosphorylation, tricarboxylic acid (TCA) cycle, fatty acid oxidation and glucose metabolism [14]. However, in addition to overlapping gene activation there is also ample evidence that ERRα and ERRγ have differential and opposing effects, which can be due to interactions with corepressors, coactivators, posttranslational modification, or differential cell expression [14]. Opposing effects for ERRα and ERRγ are seen in breast cancer [20], regulation of gluconeogenesis in the liver [20, 21], skeletal muscle function [20, 21], macrophage function [21, 22], and regulation of lactate dehydrogenase A (LDHA) related to anaerobic glycolysis [14]. Finally, ERRα and ERRγ are highly expressed in the mouse and human kidney [23, 24].

The roles of ERRα and ERRγ in modulating age-related impairment in mitochondrial function and age-related inflammation (inflammaging) are not known. We undertook our current studies to determine whether an ERR pan agonist, activating

ERRα, ERRβ, and ERRγ, would improve mitochondrial dysfunction and inflammation in the aging mouse kidney.

RESULTS

ERRα and ERRγ expression is decreased in the aging human kidney

In a previous study, we found decreased expression of ERRα and ERRγ in the aging mouse kidney and expression was upregulated by the dual FXR-TGR5 agonist INT-767 or CR. Further, increased ERR expression correlated with increased mitochondrial biogenesis and function in the treated aging kidneys [12]. In light of the role of ERR in mitochondrial biogenesis, we determined whether decreased expression also occurs in the human aging kidney. We performed immuno-histochemistry with human kidney sections from young and old individuals. The results indicate that both ERRα and ERRγ are expressed in renal tubules and that their expression levels were markedly decreased in aging human kidney (**Figure 1A**). Since ERRs are important modulators of mitochondrial biogenesis, we also stained the human kidney sections for the mitochondrial PDH e2/e3 and found a marked decrease in PDH immunostaining in the aging human kidney samples (**Figure 1B**).

Transforming growth factor (TGF)-β and tumor necrosis factor (TNF)-α expression are increased in the aging kidney (**Supplementary Figure 1**). Thus, we were interested to determine whether TGF-β and TNF-α at least in part mediate the decreased expression of ERR in the kidney. We found that in cultured human primary proximal tubules, TGF-β significantly decreased expression level of ERRγ mRNA while ERRα was unaffected. Expression of PGC1α and Mcad (encoding medium chain acyl-CoA dehydrogenase)

were decreased as well in TGF-β treated cells (**Figure 1C**). TNF-α also had a similar effect to decrease ERRγ expression (**Figure 1C**).

ERRα and ERRγ RNA distribution in the mouse kidney

To determine where ERRα and ERRγ mRNA are expressed in the mouse kidney, we performed single nuclei RNAseq [25, 26]. With 3000-5000 nuclei sequenced at 100k read depth, 12 expression clusters were identified and assigned to major cell types in the mouse kidney (**Figure 2A**). We found that ERRα was expressed mostly in proximal tubules, intercalated cells and podocytes. ERRγ was expressed mostly in proximal tubules and intercalated cells (**Figure 2B**). Compared to young kidneys, S1/S2 segments of aging proximal tubules show a decline in ERRα and ERRγ expression (**Figure 2C**).

Pan ERR agonist treatment improves the age-related kidney injury

Since the main known role of ERRs is to regulate mitochondrial function, we sought to treat the aging mice with a recently available pan ERR agonist. We found that 2-month treatment of 21-month-old mice has significantly improved the age-related increased albuminuria, associated with decreased kidney weight following the treatment (**Figure 3A**). The change in albuminuria is believed to be related to improved podocyte function as the podocyte marker NPHS2 (podocin) expression is increased after the treatment (**Figure 3B**). In addition to the profibrotic markers TGF-β, PAI-1 and Col IV, the marker for macrophage infiltration F4/80, and tubular injury marker neutrophil gelatinase-associated lipocalin (NGAL) decreased with the pan-agonist treatment (**Figure 3C**).

Finally, with the cytokine profiler we found the kidney injury markers, Ngal, kidney injury marker-1 (Kim1), osteopontin and CC-motif ligand chemokine-21 (Ccl21) were increased in the aging kidney and partially normalized by pan-ERR agonist treatment (**Figure 3D**).

Pan ERR agonist treatment modulates mitochondrial metabolism and inflammation in the aging kidney

To determine the actions of the pan-ERR agonist, we examined *Esrra, Esrrb* and *Esrrg* mRNA abundance. Although they were all decreased in the kidneys of aging mice, treatment with the ERR pan-agonist induced significant increases in their expression to levels observed in the young mice (**Figure 4A**).

Next, we performed bulk RNAseq analysis to determine which pathways are affected by restored ERR expression. The main pathways downregulated in the aging kidney and upregulated by the pan ERR agonist were related to mitochondrial function (**Figure 4B**). In addition, certain immune related pathways were upregulated in the aging kidney but downregulated upon ERR treatment (**Figure 4C**). In addition to RNAseq, we performed mass-spec proteomics. The proteomics analysis further revealed that the major regulated pathways included the mitochondrial electron transport chain (ETC), TCA cycle, and mitochondrial fatty acid β-oxidation (**Figure 4D**). Using the fact that the RNAseq and the mass-spec proteomics analyses were performed on the same set of biological samples, we applied multi-omics integration using the two-way orthogonal Partial Least Squares (o2PLS) approach. We found a regulation pattern that separated

the old mice from old mice treated with pan ERR agonist. Pan-ERR agonist treatment decreased gene expression (**Figure 4E**) and protein abundance (**Figure 4F**) of pathways related to immune system activation.

As the hallmarks for aging kidneys are decreased mitochondrial function and increased inflammation [27, 28], we next determined whether treatment with the pan ERR agonist improved these specific defects in the aging kidneys.

Pan ERR agonist treatment restored mitochondrial function in aging kidneys

The canonical function of ERR is to induce mitochondrial biogenesis. We found that the pan-ERR agonist increased expression of the master mitochondrial biogenesis regulators PGC1α and PGC1β in aging kidneys. Consistently, mitochondrial transcription factor *Tfam1* expression was decreased in the aging kidney and increased with the pan-ERR agonist. As a result, mitochondrial DNA/nuclear DNA ratio was increased in aging kidneys following treatment, indicative of increased mitochondrial biogenesis (**Figure 5A**). The increased mitochondrial biogenesis was accompanied by increased expression of genes related to the mitochondrial ETC complexes, such as complex I subunit *Ndufb8*, complex II subunit *Sdhc*, complex III subunit *Uqcrb*, complex IV subunit *Cox6a2*, and complex V subunit *Atp5b* (**Figure 5B**). Native blue gel further showed increased expression of assembled mitochondrial complexes after the treatment (**Figure 5C**). This is consistent with the increased gene expression in TCA cycle, such as *Pdhb*, *Mdh1*, *Idh3b*, and *Sucla2* (**Figure 5D**). Since TCA cycle can produce NADH which is required for complex I driven mitochondrial oxidative phosphorylation, we further determined fractional intensity of free NADH with phasor

approach to fluorescence lifetime imaging microscopy (FLIM) [29, 30]. Analysis of the FLIM images showed that there was decreased free NADH fraction in aging kidneys, which suggests a lower capacity of NADH regeneration in aging kidney, in agreement with the downregulation of TCA cycle enzyme expression [31]. Treatment with the pan ERR agonist shifted the free NADH fraction in the aging kidney towards the young kidneys – in cumulative plots for all samples [30, 32] (**Figure 5E**).

The interrelationship between the ETC and TCA cycle is illustrated in **Figure 5F**. The changes in ETC complexes and TCA cycle resulted in the increased maximum respiration capacity in mitochondria isolated from treated aging kidneys (**Figure 5G**). In addition, mRNAs encoding enzymes that mediate mitochondrial fatty acid β-oxidation, including *Cpt1a* and *Mcad*, were upregulated by the pan ERR agonist (**Figure 5H**), suggesting that ERR agonism promotes mitochondrial fatty acid β-oxidation.

Pan ERR agonist treatment altered mitochondrial dynamics in aging kidneys

Transmission electron microscopy showed alterations in the mitochondria of aging kidneys, including decreases in the area, perimeter, and minimum Feret diameter in the aging kidneys; these parameters were restored to levels seen in young kidneys upon treatment with the pan ERR agonist (**Figure 5I**). Since these mitochondrial changes are reminiscent of alterations in mitochondrial fusion and fission, we also measured the expression of proteins that regulate mitochondrial fusion and fission. Mitofusin 2 (Mfn2) is found in the outer membrane that surrounds mitochondria and participates in mitochondrial fusion [33]. There was a significant decrease in Mfn2 in the aging kidney, and the ERR pan agonist increased the Mfn2 protein abundance in both the young and

the old kidneys, fully restoring levels in the old kidneys to levels of the untreated young kidneys (**Figure 5J**). Opa1 protein localizes to the inner mitochondrial membrane and helps regulate mitochondrial stability, energy output, and mitochondrial fusion [34]. While there was no significant change in the protein level in the aging kidney, upon treatment there was a tendency for the protein level to increase in the aging kidneys (**Figure 5J**). In addition, there were also significant decreases in mitoguardin 2 (*Miga2*) and mitoPLD (*Pld6*) mRNA levels in the aging kidneys that were normalized upon treatment with the pan-ERR agonist (**Figure 5J**). Mitoguardin 2 regulates mitochondrial fusion through mitoPLD [35]. Drp1, is a member of the dynamin superfamily of proteins and is a fundamental component of mitochondrial fission [33]. There were significant increases in Drp1 and phospho-Drp1 protein in the kidneys of aging mice, which were restored to levels seen in young mice following treatment with the pan ERR agonist (**Figure 5J**).

Pan ERR agonist treatment decreased inflammation in aging kidneys

Mitochondria are immunogenic organelles and mitochondrial dysfunction generates several immunogenic molecules, including mtDNA [36] and mtRNA. The cyclic GMP-AMP synthase (cGAS)-stimulator of interferon genes (STING) has been reported as one of the innate immune receptors to be activated by mtDNA leaking into cytosol [37, 38]. In the aging kidneys, we found increased expression of STING and cGAS mRNA and protein level, which was significantly decreased by treatment with the ERR pan agonist (**Figure 6A**). We also reported the similar changes found with RNA sensors RIG-I/MDA5/LGP2 and other nucleic acid sensors like TLRs [39, 40] (**Figure 6B**). We further examined the downstream response and we found out that expression of mRNA encoding components in NFκB signaling pathway (*Rel, RelB, Nfkb2*, and p65 protein) were

increased in the aging kidney, but that pan-ERR agonist treatment decreased NFκB signaling (**Figure 6C**).

In addition, we examined another potential STING-activated interferon signaling pathway and observed the corresponding changes in STAT3 (**Figure 6C**). As a marker for STAT3 activation, we found a significant increase in both p-Tyr705-STAT3 protein and total STAT3 protein, this increase was substantially suppressed upon treatment with the pan-ERR agonist. This cascade signaling activation was in parallel to the expression of senescence marker p21, which was induced in the aging kidney and reduced by the treatment with the pan-ERR agonist (**Figure 6D**). Another senescence marker, p16, was increased in the aging kidneys but was unaffected by the treatment (**Figure 6D**). Both of these cellular senescence markers are downregulated in aging kidneys with life-long CR (**Supplementary Figure 2**).

To determine which senescence associated secretory phenotype (SASP) factors are regulated by the pan-ERR agonist treatment in the aging kidney, we searched the RNAseq data and verified by real-time PCR that RNAs encoding the proinflammatory cytokines IL-1β and TNF-α, chemokine receptor CCR5, the metallopeptidase inhibitor TIMP1, and the cell adhesion molecule ICAM1 were increased in the aging kidney and treatment with the pan-ERR agonist decreased their expression (**Figure 6D**).

STING inhibitor decreased inflammation and increased mitochondrial gene expression in aging kidneys

To determine if the increase in STING mRNA and protein per se mediates age-related increase in inflammation, we used a known STING inhibitor C-176 [41] to treat the aging mice. C-176 decreased IL-1β, Stat3 and the senescence marker p21 expression in the

aging kidney (**Figure 7A**). Unexpectedly, we found the expression of master regulator for mitochondria biogenesis PGC1α and PGC1β in aging kidney were also increased with the treatment, along with ERRα (**Figure 7B**). Genes involved in mitochondrial ETC complex, Ndufs1, Cox6a2, and ATP5e, and fatty acid oxidation gene Mcad were also found upregulated by STING inhibitor (**Figure 7B**).

DISCUSSION

The data presented here have identified the nuclear hormone receptors the estrogen related receptors ERRα, ERRβ, and ERRγ as important modulators of age-related mitochondrial dysfunction and inflammation. ERRα, ERRβ, and ERRγ expression is decreased in the aging kidney, and lifelong CR results in increases in expression of ERRα, ERRβ, and ERRγ in the kidney. In parallel, CR also prevents age-related mitochondrial dysfunction and inflammation [12, 42, 43]. ERRs therefore act as potential CR mimetics in the kidney. Remarkably, only a 4-week treatment of 21-month-old mice with the pan ERR agonist reversed the age-related increases in albuminuria and podocyte loss, mitochondrial dysfunction and inflammation. These effects were comparable with those achieved with lifelong CR, which is known to protect against age-related co-morbidities, including loss of renal function [10, 11, 42].

Recent evidence indicates that mitochondrial dysfunction is one of the mediators of cellular senescence, and the associated SASP includes pro-inflammatory cytokines and pro-fibrotic growth factors [44, 45]. This process may also be involved in the age-related inflammation, termed inflammaging or senoinflammation, which is also prevented by CR [46, 47].

Mitochondrial dysfunction has recently been linked to activation of the cGMP-AMP synthase (cGAS)-stimulator of interferon genes (STING) signaling pathway, which plays key roles in immunity, inflammation, senescence and cancer [37, 38, 48, 49]. In addition to the recent identification of the importance of this signaling pathway in mouse models of acute kidney injury, chronic kidney disease and fibrosis [38, 50], our studies also show

increased expression of STING in aging kidneys, and its downregulation following treatment with the pan ERR agonist.

In addition to cGAS-STING signaling, mitochondrial dysfunction is also associated with activation of STAT3 [51]. Increased STAT3 signaling is associated with senescence [52] as well as kidney disease [53]. We found increased STAT3 in the aging kidneys both at the mRNA and protein level, including increased phospho-STAT3 (Tyr^{705}) and normalization after treatment with the pan ERR agonist.

To determine whether STING activation can mediate aging-related inflammation, we treated aging mice with STING inhibitor. We found that STING inhibition decreased inflammation in aging kidney, as reported in other models using STING inhibitor or STING knockout mice [38, 50]. However, we found that STING inhibition can further increase mitochondrial gene expression, suggesting a model where mitochondrial injury triggers inflammation, adding forward feedback on mitochondrial dysfunction in aging kidney. It has been consistent with the findings of mitochondrial damage in acute kidney injury induced by lipopolysaccharide, an endotoxin that activate innate immunity (via TLR4) to induce circulation cytokines [54-56].

At this time, it is not known whether the pan-ERR-induced decreases in STING and STAT3 in the aging kidney mediate the decreases in IL-1β, ICAM1 and Timp1. However, our studies identify the ERRs as beneficial modulators of mitochondrial dysfunction and inflammation in the aging kidney.

EXPERIMENTAL PROCEDURES

Mice: Studies were performed in 4-month-old and 21-month-old male C57BL/6 male mice obtained through the NIA aging rodent colony. Mice received 3% DMSO vehicle or the pan ERR agonist SLU-PP-332 (unpublished data from Dr. Burris lab) at a dose of 25 mg/kg body weight/day, administered intraperitoneally. Mice were dosed for 8 weeks, following which they underwent euthanasia and the kidneys were harvested and processed for a) histology, b) transmission electron microscopy, c) isolation of nuclei, d) isolation of mitochondria, and e) biochemical studies detailed below. Another cohort of male C57BL/6 mice with the same age were received the same vehicle as above or C-176 (Focus Biomolecules, Plymouth Meeting, PA) at a dose of 1mg/kg body weight/day with intraperitoneal injection. This treatment lasted for 3 weeks.

Immunohistochemistry: Formalin-fixed paraffin-embedded tissue sections were subjected to antigen retrieval with EDTA buffer in high pressure heated water bath and staining was performed using either mouse monoclonal ERRα (1:2500, Abcam, Cambridge, MA) or ERRγ (1:400, Abcam) antibodies for 90 minutes or pyruvate dehydrogenase (PDH) E2/E3bp (1:1000, Abcam) antibody for 45 minutes. Then UnoVue HRP secondary antibody detection reagent (Diagnostic BioSystems, Pleasanton, CA) was applied followed by DAB chromogen. The imaging was done with Nanozoomer (Hamamatsu Photonics, Japan).

Cell culture: Primary human proximal tubule epithelial cells (cat#: PCS-400-010) were purchased from ATCC (Manassas, VA). Cells were cultured in Renal Epithelial Cell Basal Medium (ATCC cat#: PCS-400-030) supplemented with Renal Epithelial Cell Growth Kit (ATCC cat#: PCS-4000-040) at 37°C in 5% CO2. Cells were cultured to 70-80% confluence and then treated with vehicle (4mM HCl with 0.1% bovine serum albumin) or 10 ng/mL TGF-β1 (Cat#: 7754-BH-005, R&D Systems, Minneapolis, MN) or 10 ng/mL TNF-α (Cat#210-TA-020, R&D Systems) for 24 hours. Cells were then harvested and analyzed for gene expression.

Transmission Electron Microscopy: One mm^3 cortex kidney tissues were fixed for 48 hrs. at 4^oC in 2.5% glutaraldehyde and 1% paraformaldehyde in 0.1M cacodylate buffer (pH 7.4) and washed with cacodylate buffer three times. The tissues were fixed with 1% OsO_4 for two hours, washed again with 0.1M cacodylate buffer three times, washed with water and placed in 1% uranyl acetate for one hour. The tissues were subsequently serially dehydrated in ethanol and propylene oxide and embedded in EMBed 812 resin (Electron Microscopy Sciences, Hatfield, PA). Thin sections, approx. 80 nm, were obtained by utilizing the Leica ultracut-UCT ultramicrotome (Leica, Deerfield, IL) and placed onto 300 mesh copper grids and stained with saturated uranyl acetate in 50% methanol and then with lead citrate. The grids were viewed with a JEM-1200EXII electron microscope (JEOL Ltd, Tokyo, Japan) at 80kV and images were recorded on the XR611M, mid mounted, 10.5M pixel, CCD camera (Advanced Microscopy Techniques Corp, Danvers, MA). Mitochondrial morphology was assessed with ImageJ software by manually tracing all mitochondria that were completely within the field of

view in 6 random images from each mouse (n = 3-4 each group). The area, perimeter, and minimum Feret diameter of each mitochondrion were measured.

Autofluorescence FLIM: autofluorescence FLIM signals were acquired using an Olympus FVMPERS microscope (Waltham. MA) equipped with the DIVER (Deep Imaging via Enhanced-Photon Recovery) detector - developed at the Laboratory for Fluorescence Dynamics (LFD), University of California at Irvine, CA, and FLIMbox (ISS, Champaign, IL) for phasor lifetime acquisition, **as detailed in Supplementary Methods**.

RNA extraction and real-time quantitative PCR: Total RNA was isolated from the kidneys using Qiagen RNeasy mini kit (Valencia, CA), and cDNA was synthesized using reverse transcript reagents from Thermo Fisher Scientific (Waltham, MA). Quantitative real-time PCR was performed as previously described [57], and expression levels of target genes were normalized to 18S level. Primer sequences are listed in **Supplementary Table 1**.

Bulk RNA-seq: Approximately 300-500ng of kidneys RNA were used to generate barcoded RNA libraries using Ion AmpliSeq Transcriptome Mouse Gene Expression Panel, Chef-Ready Kit. Library quantification was performed using the Ion Library Quantitation Kit (Thermo Fisher Scientific). Sequencing was done on an Ion Proton with signal processing and base calling using Ion Torrent Suite (Thermo Fisher Scientific). Raw reads were mapped to Ampliseq supported mm10 transcriptome. Quality control

metrics and normalized read counts per million were generated using the RNA-seq Analysis plugin (Ion Torrent Community, Thermo Fisher Scientific).

Single nuclei RNA-seq: Mouse kidney single nuclei were isolated [25, 26] and counted using the EVE Automated Cell Counter (NanoEnTek, VWR, Radnor, PA). The resulting mixture was provided to the Genomics and Epigenomics Shared Resource (GESR) at Georgetown University, and further processed by the Chromium Controller (10X Genomics, Pleasanton, CA) using Single Cell 3' GEM Kit v3, Single Cell 3' Library Kit v3, i7 multiplex kit, Single Cell 3' Gel Bead Kit v3 (10X Genomics) according to the manufacturer's instructions with modifications for single nuclei. Libraries were sequenced on the Illumina Novaseq S4 System (Illumina, San Diego, CA) to an average depth of >300 M reads PF per sample. Data Analysis: The 10X Genomics BCL data was loaded into the Cellranger Makefastq pipeline, which demultiplexes raw BCL files generated by Illumina sequencer into FASTQ files which were further analyzed by the Cellranger Count pipeline. Inside the Cellranger Count pipeline, the STAR algorithm was used to align sequencing reads to the Mouse mm10 genome reference. The Cloupe files were obtained and were further visually investigated by the Loupe Cell Browser.

Proteomics: 200 microgram of kidney tissue were homogenized and lysed by 8M urea in 20mM HEPES (pH=8.0) buffer with protease and phosphatase inhibitors using Tissue Lyser II (QIAGEN). Samples were reduced and alkylated followed by MS-grade trypsin digestion. The resulting tryptic peptides were labeled with 11 plex tandem mass tag

(TMT). After quench, the tagged peptides were combined and fractionated with basic-pH reverse-phase high-performance liquid chromatography, collected in a 96-well plate and combined for a total of 12 fractions prior to desalting and subsequent liquid chromatography−tandem mass spectrometry (LC−MS/MS) processing on a Orbitrap Q-Exactive HF (Thermo Fisher Scientific) mass spectrometer interfaced with an Ultimate 3000 nanoflow LC system [58]. Each fraction was separated on a reverse phase C_{18} nano-column (25μm × 75cm, 2μm particles) with a linear gradient 4~45% solvent B (0.1% TFA in Acetonitrile). Data dependent mode was applied to analyze the top 15 most abundant peaks in one acquisition cycle.

MS raw files were mapped against Uniprot mouse database (version 20170207) using the MaxQuant software package (version 1.5.3.30) with the Andromeda search engine . Corrected intensities of the reporter ions from TMT labels were obtained from the MaxQuant search. For the TMT experiment, relative ratios of each channel to the reference channel (channel11, pooled from 20 samples) were calculated. Perseus (version 1.5.5.3) was used to further analyze and visualize the data. Hierarchical clustering of proteins was obtained in Perseus using log ratios or log intensities of protein abundance.

Mitochondrial isolation: Kidney mitochondria were isolated using the kit from Sigma (St. Louis, MO) according to manufacturer instructions.

Mitochondrial Biogenesis: We measured mitochondrial (*Cytb*) and nuclear (*H19*) DNA by RT-QPCR.

Mitochondrial Respiration: We measured basal respiration, ATP turnover, proton leak, maximal respiration and spare respiratory capacity using the *Seahorse* XF96 Analyzer on equally loaded freshly isolated kidney mitochondria. We also measured mitochondrial complex I, II, III, IV, and V protein abundance by Native Blue Gel Electrophoresis (Thermo Fisher Scientific) with equally loaded mitochondrial fractions.

Multi-omics data analysis and integration bioinformatics methods: The project includes several types of omics data (proteomics, transcriptomics, and metabolomics) measured in the same set of biological samples. Taking advantage of the multi-omics set of measurements reflecting the same biological processes in the samples from different perspectives, we performed Two-way Orthogonal Partial Least Square (O2PLS) integration [59] in pairs of the transcriptomic, proteomic, and metabolomic datasets. As a result of each omics pair integration, matching orthogonal components in dataset-members show major mutually coordinated regulations in this particular pair of the omics datasets.

The majority of the gene expression and protein abundance profiles can be presented as combinations in different proportions of three major o2PLS components. An association of a gene or protein profile with one of individual components is defined by “loading” of its profile on this particular component and determining how high the projection of the profile is on the component where both are sequences of per-sample

values. Subsets of genes and proteins most associated with individual components were determined.

Western blotting: Western blotting was performed as previously described [57, 60-62]. Equal amount of total protein was separated by SDS-PAGE gels and transferred onto PVDF membranes. After HRP-conjugated secondary antibodies, the immune complexes were detected by chemiluminescence captured on Azure C300 digital imager (Dublin, CA) and the densitometry was performed with ImageJ software. Primary antibodies used for western blotting were listed in **Supplementary Table 1**.

Cytokine arrays: Cytokines in 200 microgram kidney lysate (pooled from 5-6 samples with equal amount of protein) were detected with the Proteome Profiler Array (ARY028; R&D Systems) according to manufacturer's instructions.

Statistical analysis: Results are presented as the means ± SEM for at least three independent experiments. Following the Grubbs' outlier test, the data were analyzed by ANOVA and Newman–Keuls tests for multiple comparisons or by *t* test for unpaired data between two groups (Prism 6, GraphPad, San Diego, CA). Statistical significance was accepted at the $P<0.05$ level.

Study approval: Animal studies and relative protocols were approved by the Animal Care and Use Committee at the Georgetown University. All animal experimentation was

conducted in accordance with the Guide for Care and Use of Laboratory Animals (National Institutes of Health, Bethesda, MD).

FIGURE LEGENDS

Figure 1. ERRα, ERRγ, and PDH expression is decreased in the aging human kidney. **A)** ERRα and ERRγ immunohistochemistry on kidney sections from young and old subjects. The nuclear positive staining for ERRα or ERRγ is decreased in old kidney sections. **B)** PDH immunohistochemistry on kidney sections from young and old subjects. PDH staining is decreased in old kidney sections. **C)** TGF-β treated human primary proximal tubules significantly decreased expression level of ERRγ mRNA but not ERRα. PGC1α and Mcad gene expression were decreased as well in TGF-β treated cells. TNF also had a similar effect to decrease ERRγ expression. N=3 for each group. *** p< 0.001.

Figure 2. Single nuclei RNAseq of young and old kidneys. **A)** The t-distributed stochastic neighbor embedding (tSNE) shows that, with 100k read depth and 3000-5000 nuclei sequenced, we were able to identify 12 clusters and assigned them to major cell types known in the mouse kidney. **B**) We found most ERRα is expressed in proximal tubules, intercalated cells and podocytes. For ERRγ**,** we found proximal tubules and intercalated cells express most of it. The cells with positive expression of ERRα or ERRγ were labeled purple. **C)** Table to show percentage of positive expressed cells in each cluster. Compared to the young kidneys, aging proximal tubules at S1/S2 show decline in ERRα and ERRγ expression. Pod: podocyte; MC: mesangial cell; EC: endothelial cell; Mϕ: macrophage; DCT, distal convoluted tubule; LH, loop of Henle; IC: intercalated cell; CD-PC, collecting duct-principal cell; PT, proximal tubule.

Figure 3. Pan ERR agonist improved age-related renal injury. **A)** Albuminuria and kidney weight (normalized with whole body weight) were increased in aging kidneys and decreased with the treatment. N=5-6 for each group**. B)** NPHS2 (podocin) immunohistochemistry on kidney sections. Pan ERR agonist treatment reversed the decreased NPHS2 staining in aging kidneys. Scalar bar: 50 μm. N=5-6 for each group**. C)** Kidney injury markers TGF-β, PAI-1, Col4a1, F4/80, and NGAL mRNA expression are increased in aging kidneys but decreased with the treatment. N=5-6 for each group. **D)** Cytokine array showed 4 major spots that correspond to kidney injury markers Ngal, Kim1, Osteopontin and Ccl21, with increased expression in the aging kidney and decreased expression following the pan agonist treatment. Each group has one sample pooled from n=4 animals.

Figure 4. RNAseq and proteomics of kidney from old mice treated with vehicle or the pan ERR agonist. **A)** ERRα, ERRβ and ERRγ mRNA expression were decreased in the aging mouse kidneys. Treatment with the pan ERR agonist restores the mRNA levels of ERRα, ERRβ and ERRγ to levels seen in young kidneys. N=5-6 for each group. **B)** Enriched pathway analysis of RNAseq data showed that pan ERR agonist increased expression of genes related to metabolism, TCA cycle, oxidative phosphorylation and ETC, which were decreased in the untreated aging kidneys compared to the young kidneys. **C)** Enriched pathway analysis of RNAseq data showed that expression of genes related to inflammation, cytokine signaling, and innate immune system were increased in the aging kidneys and decreased with the treatment. **D)** Enriched pathway analysis of proteomics data showed that pan ERR agonist increased abundance of

proteins related to metabolism, ETC, and fatty acid β-oxidation. **E, F)** The multi-omics integration using O2PLS demonstrated a regulation pattern that separated old group from old with pan ERR agonist treatment group. Pan ERR agonist treatment decreased pathways related to immune system activation in both gene expression **(E)** and protein abundances **(F)**.

Figure 5. Pan ERR agonist treatment restored mitochondrial function in aging kidneys. **A)** Pan ERR agonist treatment in old mice increased the expression of PCG1α and PGC1β, coregulators of ERRs and mediators of mitochondrial biogenesis. The expression of the mitochondrial transcription factor Tfam1 was decreased in the kidneys of old mice and pan ERR agonist treatment restored it to levels seen in young mice. Mitochondria to nuclear DNA ratio was decreased in the kidneys of old mice and pan ERR agonist treatment restored it to levels seen in young mice, indicative of increased mitochondrial biogenesis. N=5-6 for each group. **B)** mRNA expression levels of subunits for mitochondrial ETC complex was decreased in the kidneys of old mice and pan ERR agonist treatment restored it to levels seen in young mice, indicative of improvement in ETC. N=5-6 for each group. **C)** Native blue gel indicates the increased level of assembled complex I, II, III, IV and V in the kidneys of old mice after treatment with the pan ERR agonist. N=4 for each group. **D)** mRNA expression levels of the TCA cycle enzymes were decreased in the kidneys of old mice and recovered by pan ERR agonist treatment to levels seen in young mice, indicative of restoration of the TCA cycle. One of the TCA cycle intermediates, succinic acid showed increased level in the kidneys of old mice treated with the pan ERR agonist. N=5-6 for each group. **E)**

Autofluorescence intensity (NADH channel) (top) and Phasor mapped FLIM image (bottom) on the kidney section. The phasor mapped FLIM images were pseudo colored based on the fractional intensity of the free NADH – as shown in the color scale. The fractional intensity contributions were calculated by resolving the phasor signatures from these images in between the phasor positions of free and bound NADH. Fractional intensity of NADH plot showed that there was decreased free NADH fraction in aging kidneys and the pan ERR agonist treatment shifted to more free NADH fraction. N=5-6 for each group. **F)** Interrelationship of the TCA cycle and ETC. **G)** Maximum respiration capacity in mitochondria isolated from the kidneys showed a significant impairment in old mice, which is restored to levels seen in young mice after treatment with the pan ERR agonist. N=5-6 for each group. **H)** The fatty acid β-oxidation enzymes *Cpt1a* and *Mcad* mRNA levels were decreased in the kidneys of old mice, which are restored to levels seen in young mice after treatment with the pan ERR agonist. N=5-6 for each group. **I)** Transmission electron microscopy showed alterations in the mitochondria of aging kidneys including decreases in the area, perimeter, and minimum Feret diameter, which were restored to levels seen in young kidneys upon treatment with the pan ERR agonist. N = 3-4 for each group. **J)** There was a significant decrease in mitofusin 2 protein abundance in the old kidneys and the ERR pan agonist increased the protein abundance in both the young and the old kidneys, with the resulting levels in the old kidneys being the same as in the young kidneys. In contrast, there was no significant change in the protein level of Opa1 in the old kidneys. However, upon treatment with the pan ERR agonist, there was a tendency for the protein level to increase in the aging kidneys. There were also significant decreases in mitoguardin 2 and MitoPLD mRNA

levels in the aging kidneys that were normalized upon treatment with the pan ERR agonist. In addition, there were significant increases in Drp1 and phospho-Drp1 protein in the kidneys of old mice, which were restored back to levels seen in young mice following treatment with the pan ERR agonist. N=5-6 for each group in mRNA level analysis. N=4 for each group in protein analysis.

Figure 6. Pan ERR agonist treatment decreased inflammation in aging kidneys. **A)** There were significant increases in STING and cGAS mRNA and protein level in the kidneys of old mice. Treatment with the pan ERR agonist decreases their expression in the kidneys of old mice. N=5-6 for each group in mRNA level analysis. N=4 for each group in protein analysis. **B)** RIG-I-like receptors (RIG-I, MDA5, LGP2) and toll like receptors (TLR3, 7 and 9) mRNA levels were increased in the aging kidney and decreased with the treatment. N=5-6 for each group. **C)** There were significant increases in *Rel, Relb* and *Nfkb2* mRNA, and total p65 protein expression in the kidneys of old mice and treatment with the pan ERR agonist decreased their expression to levels seen in the kidneys of young mice. There were also similar changes to *Stat3* mRNA, and p-Tyr705-STAT3 and total STAT3 protein expression. N=5-6 for each group in mRNA level analysis. N=3-4 for each group in protein analysis. **D)** There were significant increases in the cellular senescence marker p21 and p16 in the aging kidney and the pan agonist treatment reduced the level of p21 expression but not p16. As senescence associated secretory phenotype marker, *Il1b, Icam1, Timp1, Tnfa,* and *Ccr5* mRNA were found increased in the kidneys of old mice and treatment with the pan ERR agonist decreased their expression. N=5-6 for each group.

Figure 7. Treatment of aging mice with STING inhibitor C-176. **A)** STING inhibitor decreased IL-1β, Stat3, phospho-Stat3, and p21 expression in aging kidneys. N=4 for each group. **B)** STING inhibitor increased expression of PGC1α, PGC1β, ERRα, Ndufs1(complex I), Cox6a2 (complex IV), Atp5e (complex V), and MCAD in aging kidneys. N=4 for each group.

ACKNOWLEDGEMENTS

The above study is supported by NIA R01 AG049493 and NIDDK R01 DK116567 to M.L. and AHA postdoctoral fellowship to K.M. (19POST34381041) and A.E. L. (19POST34430001). J.B.K. is supported by the NIDDK Intramural Research Program.

AUTHOR CONTRIBUTIONS

This study was conceived and led by M.L. and X.X.W. X.X.W. performed most of the work. K.M. assisted with the animal studies and biochemical analysis. Y.Q. and U.G. performed the proteomics and assisted with the analysis. J.P. A.T., V.S., B.O., and L.B. performed the multi-omics processing and integration analyses. S.R. and K.B. conducted the FLIM imaging and analysis. P.D. and A.Z.R. performed the immunohistochemistry and analysis. A.E.L. performed human primary cell culture work. P.Z. and J.B.K. performed the EM and B.A.J., K.B. and A.Z.R. assisted with the data analysis. T.B. provided the reagent pan-ERR agonist. X.X.W. and M.L. wrote the manuscript with editorial input from all authors.

COMPETING INTERESTS

The authors declare no competing interests.

DATA AVAILABILITY STATEMENT

The data that support the findings of this study are available from the corresponding author upon reasonable request. RNAseq reads for all samples used in the paper have been deposited in NCBI GEO database.

REFERENCES

1. Tonelli, M, Riella, M: Chronic kidney disease and the aging population. *American journal of physiology Renal physiology,* 306: F469-472, 2014.
2. Choudhury, D, Levi, M: Kidney aging--inevitable or preventable? *Nature reviews Nephrology,* 7: 706-717, 2011.
3. Hommos, MS, Glassock, RJ, Rule, AD: Structural and Functional Changes in Human Kidneys with Healthy Aging. *Journal of the American Society of Nephrology : JASN,* 28: 2838-2844, 2017.
4. Berg, UB: Differences in decline in GFR with age between males and females. Reference data on clearances of inulin and PAH in potential kidney donors. *Nephrology, dialysis, transplantation : official publication of the European Dialysis and Transplant Association - European Renal Association,* 21: 2577-2582, 2006.
5. Tauchi, H, Tsuboi, K, Okutomi, J: Age changes in the human kidney of the different races. *Gerontologia,* 17: 87-97, 1971.
6. Fliser, D, Franek, E, Joest, M, Block, S, Mutschler, E, Ritz, E: Renal function in the elderly: impact of hypertension and cardiac function. *Kidney international,* 51: 1196-1204, 1997.
7. Jang, JY, Blum, A, Liu, J, Finkel, T: The role of mitochondria in aging. *J Clin Invest,* 128: 3662-3670, 2018.
8. Shpilka, T, Haynes, CM: The mitochondrial UPR: mechanisms, physiological functions and implications in ageing. *Nat Rev Mol Cell Biol,* 19: 109-120, 2018.
9. Hansen, M, Rubinsztein, DC, Walker, DW: Autophagy as a promoter of longevity: insights from model organisms. *Nat Rev Mol Cell Biol,* 19: 579-593, 2018.
10. Jiang, T, Liebman, SE, Lucia, MS, Li, J, Levi, M: Role of altered renal lipid metabolism and the sterol regulatory element binding proteins in the pathogenesis of age-related renal disease. *Kidney Int,* 68: 2608-2620, 2005.
11. Jiang, T, Liebman, SE, Lucia, MS, Phillips, CL, Levi, M: Calorie restriction modulates renal expression of sterol regulatory element binding proteins, lipid accumulation, and age-related renal disease. *J Am Soc Nephrol,* 16: 2385-2394, 2005.
12. Wang, XX, Luo, Y, Wang, D, Adorini, L, Pruzanski, M, Dobrinskikh, E, Levi, M: A dual agonist of farnesoid X receptor (FXR) and the G protein-coupled receptor TGR5, INT-767, reverses age-related kidney disease in mice. *J Biol Chem,* 292: 12018-12024, 2017.
13. Wei, W, Schwaid, AG, Wang, X, Wang, X, Chen, S, Chu, Q, Saghatelian, A, Wan, Y: Ligand Activation of ERRalpha by Cholesterol Mediates Statin and Bisphosphonate Effects. *Cell Metab,* 23: 479-491, 2016.
14. Audet-Walsh, E, Giguere, V: The multiple universes of estrogen-related receptor alpha and gamma in metabolic control and related diseases. *Acta Pharmacol Sin,* 36: 51-61, 2015.
15. Finck, BN, Kelly, DP: PGC-1 coactivators: inducible regulators of energy metabolism in health and disease. *J Clin Invest,* 116: 615-622, 2006.
16. Fritah, A, Christian, M, Parker, MG: The metabolic coregulator RIP140: an update. *Am J Physiol Endocrinol Metab,* 299: E335-340, 2010.
17. Yamamoto, H, Williams, EG, Mouchiroud, L, Canto, C, Fan, W, Downes, M, Heligon, C, Barish, GD, Desvergne, B, Evans, RM, Schoonjans, K, Auwerx, J: NCoR1 is a conserved physiological modulator of muscle mass and oxidative function. *Cell,* 147: 827-839, 2011.
18. Tremblay, AM, Wilson, BJ, Yang, XJ, Giguere, V: Phosphorylation-dependent sumoylation regulates estrogen-related receptor-alpha and -gamma transcriptional activity through a synergy control motif. *Mol Endocrinol,* 22: 570-584, 2008.

19. Wilson, BJ, Tremblay, AM, Deblois, G, Sylvain-Drolet, G, Giguere, V: An acetylation switch modulates the transcriptional activity of estrogen-related receptor alpha. *Mol Endocrinol,* 24: 1349-1358, 2010.
20. Ariazi, EA, Clark, GM, Mertz, JE: Estrogen-related receptor alpha and estrogen-related receptor gamma associate with unfavorable and favorable biomarkers, respectively, in human breast cancer. *Cancer Res,* 62: 6510-6518, 2002.
21. Huss, JM, Garbacz, WG, Xie, W: Constitutive activities of estrogen-related receptors: Transcriptional regulation of metabolism by the ERR pathways in health and disease. *Biochim Biophys Acta,* 1852: 1912-1927, 2015.
22. Sonoda, J, Laganiere, J, Mehl, IR, Barish, GD, Chong, LW, Li, X, Scheffler, IE, Mock, DC, Bataille, AR, Robert, F, Lee, CH, Giguere, V, Evans, RM: Nuclear receptor ERR alpha and coactivator PGC-1 beta are effectors of IFN-gamma-induced host defense. *Genes Dev,* 21: 1909-1920, 2007.
23. Bookout, AL, Jeong, Y, Downes, M, Yu, RT, Evans, RM, Mangelsdorf, DJ: Anatomical profiling of nuclear receptor expression reveals a hierarchical transcriptional network. *Cell,* 126: 789-799, 2006.
24. Berry, R, Harewood, L, Pei, L, Fisher, M, Brownstein, D, Ross, A, Alaynick, WA, Moss, J, Hastie, ND, Hohenstein, P, Davies, JA, Evans, RM, FitzPatrick, DR: Esrrg functions in early branch generation of the ureteric bud and is essential for normal development of the renal papilla. *Hum Mol Genet,* 20: 917-926, 2011.
25. Park, J, Shrestha, R, Qiu, C, Kondo, A, Huang, S, Werth, M, Li, M, Barasch, J, Susztak, K: Single-cell transcriptomics of the mouse kidney reveals potential cellular targets of kidney disease. *Science,* 360: 758-763, 2018.
26. Wu, H, Kirita, Y, Donnelly, EL, Humphreys, BD: Advantages of Single-Nucleus over Single-Cell RNA Sequencing of Adult Kidney: Rare Cell Types and Novel Cell States Revealed in Fibrosis. *J Am Soc Nephrol,* 30: 23-32, 2019.
27. Haas, RH: Mitochondrial Dysfunction in Aging and Diseases of Aging. *Biology (Basel),* 8, 2019.
28. Sato, Y, Yanagita, M: Immunology of the ageing kidney. *Nature Reviews Nephrology*, 2019.
29. Ranjit, S, Malacrida, L, Stakic, M, Gratton, E: Determination of the metabolic index using the fluorescence lifetime of free and bound nicotinamide adenine dinucleotide using the phasor approach. *J Biophotonics,* 12: e201900156, 2019.
30. Ranjit, S, Malacrida, L, Jameson, DM, Gratton, E: Fit-free analysis of fluorescence lifetime imaging data using the phasor approach. *Nat Protoc,* 13: 1979-2004, 2018.
31. Yaseen, MA, Sutin, J, Wu, W, Fu, B, Uhlirova, H, Devor, A, Boas, DA, Sakadzic, S: Fluorescence lifetime microscopy of NADH distinguishes alterations in cerebral metabolism in vivo. *Biomed Opt Express,* 8: 2368-2385, 2017.
32. Aguilar-Arnal, L, Ranjit, S, Stringari, C, Orozco-Solis, R, Gratton, E, Sassone-Corsi, P: Spatial dynamics of SIRT1 and the subnuclear distribution of NADH species. *Proc Natl Acad Sci U S A,* 113: 12715-12720, 2016.
33. Pernas, L, Scorrano, L: Mito-Morphosis: Mitochondrial Fusion, Fission, and Cristae Remodeling as Key Mediators of Cellular Function. *Annu Rev Physiol,* 78: 505-531, 2016.
34. Liu, R, Chan, DC: OPA1 and cardiolipin team up for mitochondrial fusion. *Nat Cell Biol,* 19: 760-762, 2017.
35. Zhang, Y, Liu, X, Bai, J, Tian, X, Zhao, X, Liu, W, Duan, X, Shang, W, Fan, HY, Tong, C: Mitoguardin Regulates Mitochondrial Fusion through MitoPLD and Is Required for Neuronal Homeostasis. *Mol Cell,* 61: 111-124, 2016.
36. Rodriguez-Nuevo, A, Zorzano, A: The sensing of mitochondrial DAMPs by non-immune cells. *Cell Stress,* 3: 195-207, 2019.

37. Li, T, Chen, ZJ: The cGAS-cGAMP-STING pathway connects DNA damage to inflammation, senescence, and cancer. *J Exp Med,* 215: 1287-1299, 2018.
38. Chung, KW, Dhillon, P, Huang, S, Sheng, X, Shrestha, R, Qiu, C, Kaufman, BA, Park, J, Pei, L, Baur, J, Palmer, M, Susztak, K: Mitochondrial Damage and Activation of the STING Pathway Lead to Renal Inflammation and Fibrosis. *Cell Metab*, 2019.
39. Rehwinkel, J, Gack, MU: RIG-I-like receptors: their regulation and roles in RNA sensing. *Nat Rev Immunol*, 2020.
40. Majer, O, Liu, B, Barton, GM: Nucleic acid-sensing TLRs: trafficking and regulation. *Curr Opin Immunol,* 44: 26-33, 2017.
41. Haag, SM, Gulen, MF, Reymond, L, Gibelin, A, Abrami, L, Decout, A, Heymann, M, van der Goot, FG, Turcatti, G, Behrendt, R, Ablasser, A: Targeting STING with covalent small-molecule inhibitors. *Nature,* 559: 269-273, 2018.
42. Madeo, F, Carmona-Gutierrez, D, Hofer, SJ, Kroemer, G: Caloric Restriction Mimetics against Age-Associated Disease: Targets, Mechanisms, and Therapeutic Potential. *Cell Metab,* 29: 592-610, 2019.
43. Lopez-Lluch, G, Navas, P: Calorie restriction as an intervention in ageing. *J Physiol,* 594: 2043-2060, 2016.
44. Sturmlechner, I, Durik, M, Sieben, CJ, Baker, DJ, van Deursen, JM: Cellular senescence in renal ageing and disease. *Nat Rev Nephrol,* 13: 77-89, 2017.
45. Fontana, L, Nehme, J, Demaria, M: Caloric restriction and cellular senescence. *Mech Ageing Dev,* 176: 19-23, 2018.
46. Ferrucci, L, Fabbri, E: Inflammageing: chronic inflammation in ageing, cardiovascular disease, and frailty. *Nat Rev Cardiol,* 15: 505-522, 2018.
47. Bang, E, Lee, B, Noh, SG, Kim, DH, Jung, HJ, Ha, S, Yu, BP, Chung, HY: Modulation of senoinflammation by calorie restriction based on biochemical and Omics big data analysis. *BMB Rep,* 52: 56-63, 2019.
48. Ablasser, A, Chen, ZJ: cGAS in action: Expanding roles in immunity and inflammation. *Science,* 363, 2019.
49. Ng, KW, Marshall, EA, Bell, JC, Lam, WL: cGAS-STING and Cancer: Dichotomous Roles in Tumor Immunity and Development. *Trends Immunol,* 39: 44-54, 2018.
50. Maekawa, H, Inoue, T, Ouchi, H, Jao, TM, Inoue, R, Nishi, H, Fujii, R, Ishidate, F, Tanaka, T, Tanaka, Y, Hirokawa, N, Nangaku, M, Inagi, R: Mitochondrial Damage Causes Inflammation via cGAS-STING Signaling in Acute Kidney Injury. *Cell Rep,* 29: 1261-1273 e1266, 2019.
51. Hsia, HC, Hutti, JE, Baldwin, AS: Cytosolic DNA Promotes Signal Transducer and Activator of Transcription 3 (STAT3) Phosphorylation by TANK-binding Kinase 1 (TBK1) to Restrain STAT3 Activity. *J Biol Chem,* 292: 5405-5417, 2017.
52. Kojima, H, Inoue, T, Kunimoto, H, Nakajima, K: IL-6-STAT3 signaling and premature senescence. *JAKSTAT,* 2: e25763, 2013.
53. Bienaime, F, Muorah, M, Yammine, L, Burtin, M, Nguyen, C, Baron, W, Garbay, S, Viau, A, Broueilh, M, Blanc, T, Peters, D, Poli, V, Anglicheau, D, Friedlander, G, Pontoglio, M, Gallazzini, M, Terzi, F: Stat3 Controls Tubulointerstitial Communication during CKD. *J Am Soc Nephrol,* 27: 3690-3705, 2016.
54. Plotnikov, EY, Pevzner, IB, Zorova, LD, Chernikov, VP, Prusov, AN, Kireev, II, Silachev, DN, Skulachev, VP, Zorov, DB: Mitochondrial Damage and Mitochondria-Targeted Antioxidant Protection in LPS-Induced Acute Kidney Injury. *Antioxidants (Basel),* 8, 2019.
55. Tran, M, Tam, D, Bardia, A, Bhasin, M, Rowe, GC, Kher, A, Zsengeller, ZK, Akhavan-Sharif, MR, Khankin, EV, Saintgeniez, M, David, S, Burstein, D, Karumanchi, SA, Stillman, IE, Arany, Z, Parikh,

SM: PGC-1alpha promotes recovery after acute kidney injury during systemic inflammation in mice. *J Clin Invest,* 121: 4003-4014, 2011.

56. Cunningham, PN, Wang, Y, Guo, R, He, G, Quigg, RJ: Role of Toll-like receptor 4 in endotoxin-induced acute renal failure. *J Immunol,* 172: 2629-2635, 2004.
57. Wang, XX, Edelstein, MH, Gafter, U, Qiu, L, Luo, Y, Dobrinskikh, E, Lucia, S, Adorini, L, D'Agati, VD, Levi, J, Rosenberg, A, Kopp, JB, Gius, DR, Saleem, MA, Levi, M: G Protein-Coupled Bile Acid Receptor TGR5 Activation Inhibits Kidney Disease in Obesity and Diabetes. *J Am Soc Nephrol,* 27: 1362-1378, 2016.
58. Zhang, X, Nguyen, KD, Rudnick, PA, Roper, N, Kawaler, E, Maity, TK, Awasthi, S, Gao, S, Biswas, R, Venugopalan, A, Cultraro, CM, Fenyo, D, Guha, U: Quantitative Mass Spectrometry to Interrogate Proteomic Heterogeneity in Metastatic Lung Adenocarcinoma and Validate a Novel Somatic Mutation CDK12-G879V. *Mol Cell Proteomics,* 18: 622-641, 2019.
59. Bouhaddani, SE, Uh, HW, Jongbloed, G, Hayward, C, Klaric, L, Kielbasa, SM, Houwing-Duistermaat, J: Integrating omics datasets with the OmicsPLS package. *BMC Bioinformatics,* 19: 371, 2018.
60. Jiang, T, Wang, XX, Scherzer, P, Wilson, P, Tallman, J, Takahashi, H, Li, J, Iwahashi, M, Sutherland, E, Arend, L, Levi, M: Farnesoid X receptor modulates renal lipid metabolism, fibrosis, and diabetic nephropathy. *Diabetes,* 56: 2485-2493, 2007.
61. Wang, XX, Jiang, T, Shen, Y, Caldas, Y, Miyazaki-Anzai, S, Santamaria, H, Urbanek, C, Solis, N, Scherzer, P, Lewis, L, Gonzalez, FJ, Adorini, L, Pruzanski, M, Kopp, JB, Verlander, JW, Levi, M: Diabetic nephropathy is accelerated by farnesoid X receptor deficiency and inhibited by farnesoid X receptor activation in a type 1 diabetes model. *Diabetes,* 59: 2916-2927, 2010.
62. Wang, XX, Jiang, T, Shen, Y, Adorini, L, Pruzanski, M, Gonzalez, FJ, Scherzer, P, Lewis, L, Miyazaki-Anzai, S, Levi, M: The farnesoid X receptor modulates renal lipid metabolism and diet-induced renal inflammation, fibrosis, and proteinuria. *Am J Physiol Renal Physiol,* 297: F1587-1596, 2009.

Supplementary Table 1:

A. List of primers

Name	Forward	Reverse
Esrrα	CAGGGAGGGAAGGGATGG	ATGAGGAGAGGAGCGAAGG
Esrrb	GCACCTGGGCTCTAGTTGC	TACAGTCCTCGTAGCTCTTGC
Esrrg	AAGATCGACACATTGATTCCAGC	CATGGTTGAACTGTAACTCCCAC
Ppargc1a	GTCAGAGTGGATTGGAGTTG	AAGTCATTCACATCAAGTTCAG
Ppargc1b	TCCTGTAAAAGCCCGGAGTAT	GCTCTGGTAGGGGCAGTGA
Pdk4	AGGGAGGTCGAGCTGTTCTC	GGAGTGTTCACTAAGCGGTCA
Acadm	AACACTTACTATGCCTCGATTGCA	CCATAGCCTCCGAAAATCTGAA
Tfam1	AACACCCAGATGCAAAACTTTCA	GACTTGGAGTTAGCTGCTCTTT
mtDNA	ATAACCGAGTCGTTCTGCCAAT	TTTCAGAGCATTGGCCATAGAA
Sdhc	GCTGCGTTCTTGCTGAGACA	ATCTCCTCCTTAGCTGTGGTT
Atp5b	GGTTCATCCTGCCAGAGACTA	AATCCCTCATCGAACTGGACG
Pdhb	AGGAGGGAATTGAATGTGAGGT	ACTGGCTTCTATGGCTTCGAT
Mdh1	TTCTGGACGGTGTCCTGATG	TTTCACATTGGCTTTCAGTAGGT
Idh3b	TGGAGAGGTCTCGGAACATCT	AGCCTTGAACACTTCCTTGAC
Sucla2	ACCCTTTCGCTGCATGAATAC	CCTGTGCCTTTATCACAACATCC
Cpt1a	CTCCGCCTGAGCCATGAAG	CACCAGTGATGATGCCATTCT
Ndufb8	TGTTGCCGGGGTCATATCCTA	AGCATCGGGTAGTCGCCATA
Opa1	CGACTTTGCCGAGGATAGCTT	CGTTGTGAACACACTGCTCTTG
Miga2	GGAGGACTGAGGGTATGTCCA	CAAGGGCTGTGGCAAAAAGA
Pld6	ACCTGCACCGAGGCTTTAC	CATGTAGTCGCAGTCAGTGATG
Il1b	GCAACTGTTCCTGAACTCAACT	ATCTTTTGGGGTCCGTCAACT
Icam1	GTGATGCTCAGGTATCCATCCA	CACAGTTCTCAAAGCACAGCG
Stat3	AGCTGGACACACGCTACCT	AGGAATCGGCTATATTGCTGGT
Uqcrb	GGCCGATCTGCTGTTTCAG	CATCTCGCATTAACCCCAGTT
Cox6a2	CTGCTCCCTTAACTGCTGGAT	GATTGTGGAAAAGCGTGTGGT
Tmem173	GGTCACCGCTCCAAATATGTAG	CAGTAGTCCAAGTTCGTGCGA
Cdkn1a	CCTGGTGATGTCCGACCTG	CCATGAGCGCATCGCAATC

B. Antibodies

Name	Host	Source	Catalogue Number
OPA1	Mouse	BD Biosciences	612606
MFN2	Rabbit	Millipore	978-715-4321
DRP1	Mouse	Novusbio	H00010059-M01
p-DRP1 (s616)	Rabbit	Cell Signaling	3455S
Stat3	Rabbit	Cell Signaling	4904T
p-Stat3 (Y705)	Rabbit	Cell Signaling	9145T
PDH e2/e3	Mouse	Abcam	Ab110333

SUPPLEMENTARY METHODS

Autofluorescence FLIM measurements using DIVER microscope: To determine the effects of ERR activation on aging kidney, autofluorescence images from kidney slices of 5 µm thickness were measured using an Olympus microscope equipped with a DIVER (Deep Imaging via Enhanced Recovery) detector developed at the Laboratory for Fluorescence Dynamics (LFD), University of California at Irvine, CA. This microscope has a higher photon collection efficiency due to the large area detector and the photon counting nature of it enables FLIM imaging. The details of the detector construction have been described previously (1-6). The system assembled in Georgetown University is based on an Olympus FVMPERS (Olympus, Waltham, MA) upright laser scanning microscope equipped with the special DIVER detector. A short pulsed two photon laser (Insight Deep See X3, Spectra-Physics, Santa Clara, CA) is used as the excitation source. The samples were excited with a 20X 0.45NA air objective (Olympus, Waltham, MA). The sample is placed directly on top of the detector assembly input window below the objective and two-photon induced fluorescence is detected by a large area photomultiplier (PMT) (Hamamatsu R7600P-300, Campbell, CA). The detector assembly consists of a sealed chamber with the filter wheel/shutter inside and the housing with PMT. The refractive index matching liquid filled inside the housing removes loss of photons due to internal reflections and thus achieves efficient collection of photons. Two BG-39 filters serve as input and output windows of the chamber, and block NIR excitation light from entering PMT, transmitting UV and visible fluorescence and harmonic signals. The only optical elements in the detector assembly are BG-39 filters and the glass filter of the filter wheel, allowing detection of emitted photons from 320-650 nm wavelength range. The samples were excited with a 710 nm

pulsed laser and two photon autofluorescence FLIM was collected using the blue filter of the detection assembly (λ_{EM} = 410 -510 nm). Each of the images was taken with a 625 µm field of view, 20 µs pixel dwell time and 16 repeat scans for increasing signal to noise ratio.

The signal from the PMT is collected using a FLIMBox (ISS, Champaign, IL) and directly transferred to the phasor plot (Figure S1). Details of the phasor approach towards FLIM analysis has been explained elsewhere (7-10). Briefly, this method of lifetime analysis involves transferring the fluorescence intensity decays in the Fourier space and plotting the Fourier components against each other. This results in a phasor plot (Figure S1) where each point results from a pixel of the image. The autofluorescence from the tissue have a non-zero lifetime and appear inside the semicircle. A distribution in the phasor plot can then either be selected using a cursor and the images can be colored accordingly. Phasor approach towards FLIM is a fit free approach, increases the speed of the analysis, and decreases the computational difficulty associated with FLIM technique (7-11). The data collection and analysis was carried out by using SimFCS, developed by Prof. Enrico Gratton at the LFD. A continuous color scheme was used for the phasor-mapped image and the redder/ purple color represents more bound NADH and more cyan/white color represents more free NADH (Figure 4e in main text). The position of the bound NADH and free NADH are shown by red and blue cursors, respectively (12).

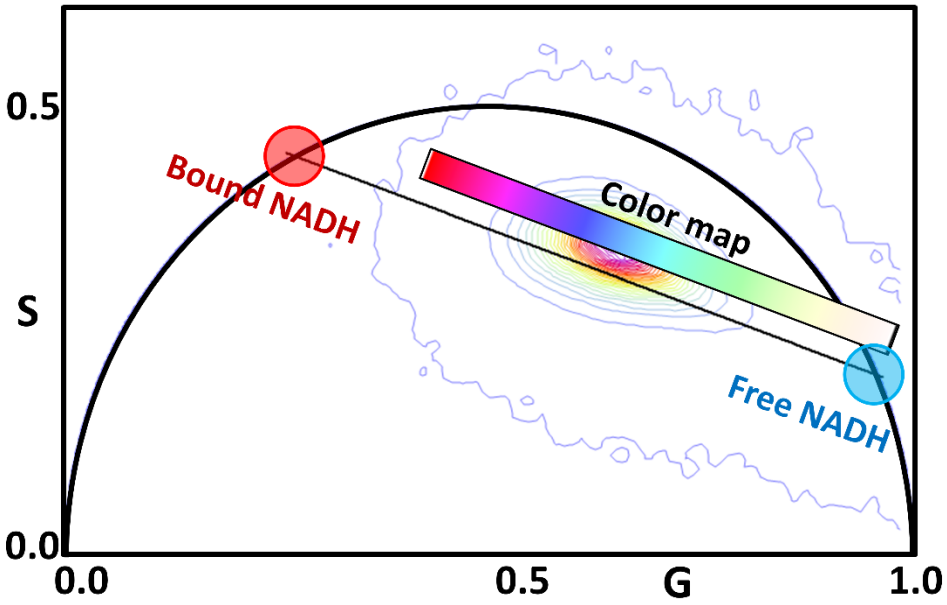

Figure S1: The phasor map showing the lifetime distribution of NADH in kidney slices. A continuous color scheme was used for the phasor-mapped image and the redder/ purple color represents more bound NADH and more cyan/white color represents more free NADH. The position of the bound NADH and free NADH are shown by red and blue cursors, respectively.

References

1. Crosignani V, Dvornikov A, Aguilar JS, Stringari C, Edwards R, Mantulin WW, Gratton E. Deep tissue fluorescence imaging and in vivo biological applications. J Biomed Opt 2012;17:116023.
2. Crosignani V, Jahid S, Dvornikov AS, Gratton E. A deep tissue fluorescence imaging system with enhanced SHG detection capabilities. Microsc Res Tech 2014;77:368-373.
3. Ranjit S, Dobrinskikh E, Montford J, Dvornikov A, Lehman A, Orlicky DJ, Nemenoff R, et al. Label-free fluorescence lifetime and second harmonic generation imaging microscopy improves quantification of experimental renal fibrosis. Kidney Int 2016;90:1123-1128.
4. Ranjit S, Dvornikov A, Levi M, Furgeson S, Gratton E. Characterizing fibrosis in UUO mice model using multiparametric analysis of phasor distribution from FLIM images. Biomed Opt Express 2016;7:3519-3530.

5. Ranjit S, Dvornikov A, Stakic M, Hong SH, Levi M, Evans RM, Gratton E. Imaging Fibrosis and Separating Collagens using Second Harmonic Generation and Phasor Approach to Fluorescence Lifetime Imaging. Sci Rep 2015;5:13378.
6. Dvornikov A, Malacrida L, Gratton E. The DIVER microscope for imaging in scattering media.
Methods Protoc. 2019; 2(2): 53. PMCID: PMC6632175
7. Stringari C, Nourse JL, Flanagan LA, Gratton E. Phasor fluorescence lifetime microscopy of free and protein-bound NADH reveals neural stem cell differentiation potential. PLoS One 2012;7:e48014.
8. Stringari C, Cinquin A, Cinquin O, Digman MA, Donovan PJ, Gratton E. Phasor approach to fluorescence lifetime microscopy distinguishes different metabolic states of germ cells in a live tissue. Proc Natl Acad Sci U S A 2011;108:13582-13587.
9. Digman MA, Caiolfa VR, Zamai M, Gratton E. The phasor approach to fluorescence lifetime imaging analysis. Biophys J 2008;94:L14-16.
10. Ranjit S, Malacrida L, Gratton E. Differences between FLIM phasor analyses for data collected with the Becker and Hickl SPC830 card and with the FLIMbox card. Microsc Res Tech. 2018; 81(9): 980-989.
11. Digman MA, Gratton E. The phasor approach to fluorescence lifetime imaging: exploiting phasor linear properties. Fluorescence Lifetime Spectroscopy and Imaging: Principles and Applications in Biomedical Diagnostics. By L Marcu, PMW French, and DS Elson (Editors). CRC Press, pp. 235-248, 2014. ISBN: 9781439861677.
12. Ranjit S, Malacrida L, Stakic M, Gratton E. Determination of the metabolic index using the fluorescence lifetime of free and bound NADH in the phasor approach. J Biophotonics. 2019; [Epub ahead of print].

Figure 1

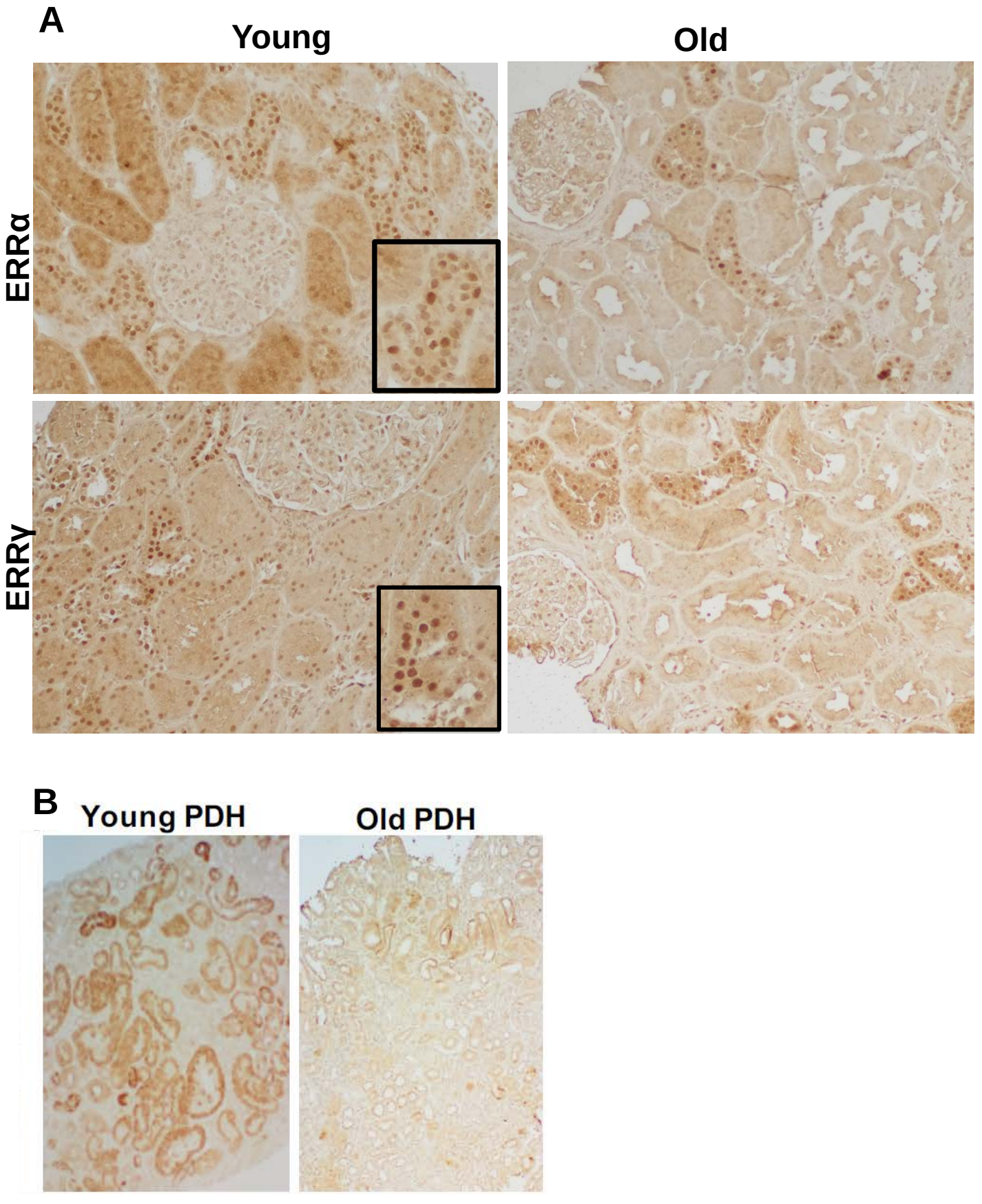

Figure 1

C

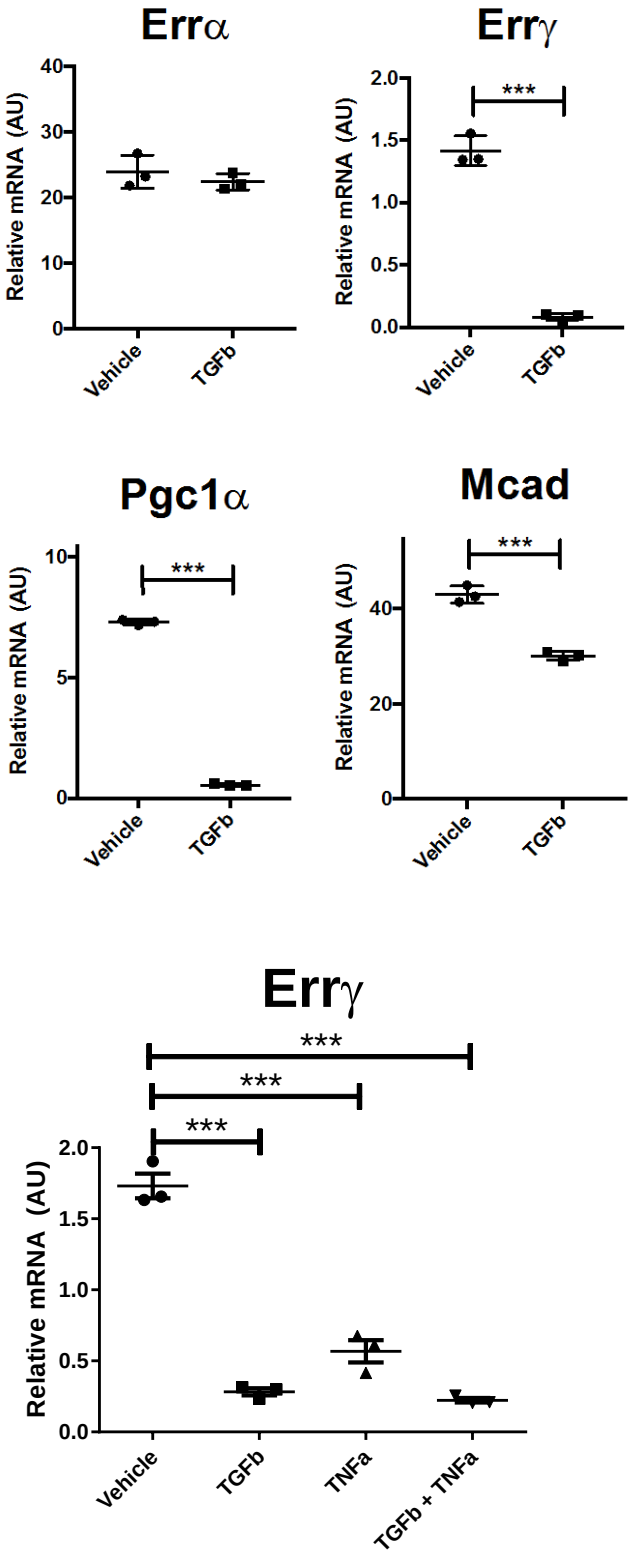
Errα
Errγ
Pgc1α
Mcad
Errγ
Relative mRNA (AU)
Vehicle
TGFb
TNFa
TGFb + TNFa
***

Figure 2

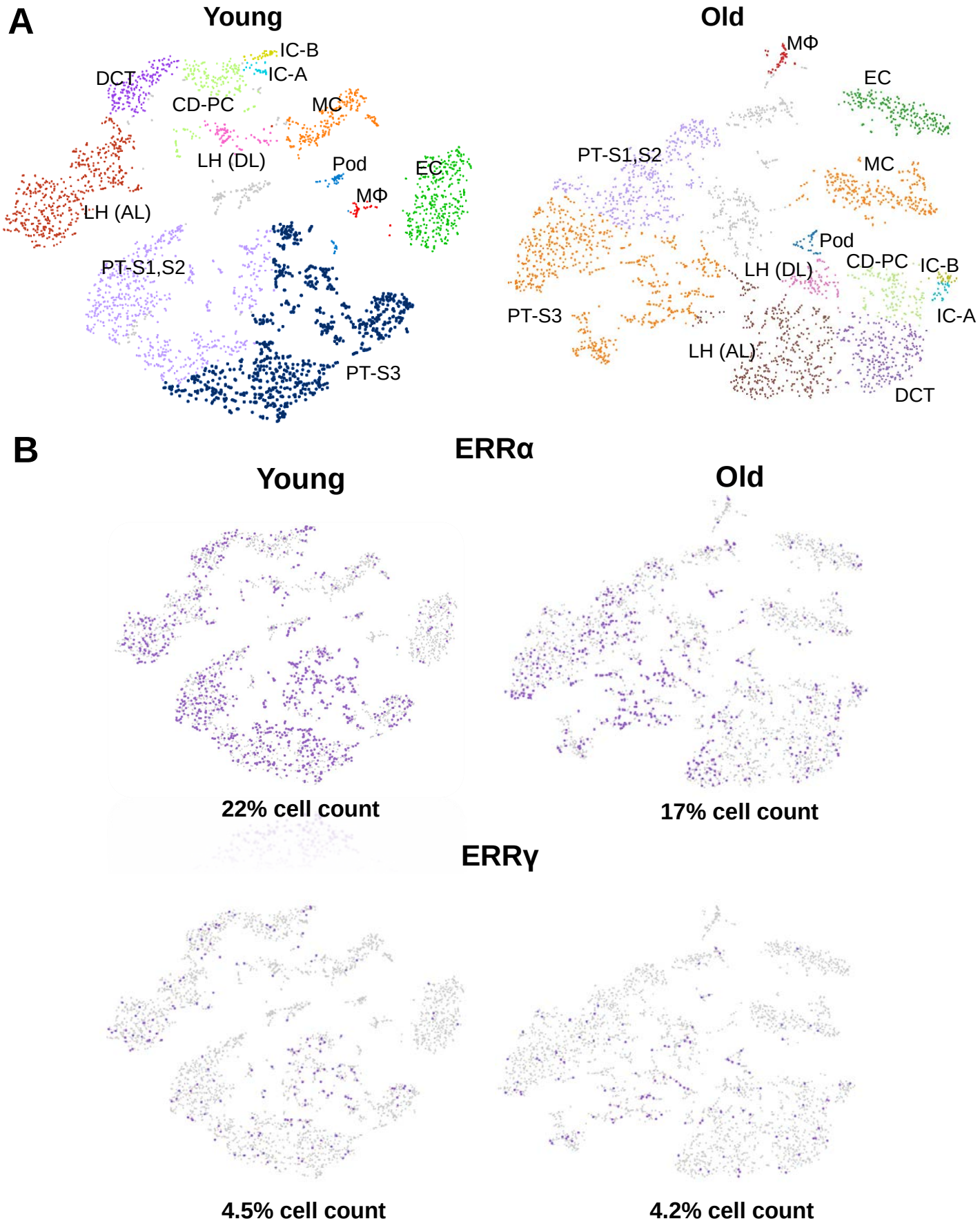
A
Young
IC-B
IC-A
DCT
CD-PC
MC
LH (DL)
Pod
EC
MΦ
LH (AL)
PT-S1,S2
PT-S3
Old
MΦ
EC
PT-S1,S2
MC
Pod
CD-PC
IC-B
LH (DL)
PT-S3
IC-A
LH (AL)
DCT
B
ERRα
Young
Old
22% cell count
17% cell count
ERRγ
4.5% cell count
4.2% cell count

Figure 2

C

% of ERRα positive cells in each cluster			
	Young	Old	
Pod	27	14	
MC	8	7	
EC	4	5	
MΦ	4	4	
DCT	15	10	
LH-AL	21	17	
LH-DL	11	8	
IC-B	41	25	
IC-A	27	12	
CD-PC	12	13	
PT-S3	32	28	
PT-S1/S2	30	19	

% of ERRγ positive cells in each cluster			
	Young	Old	
Pod	0	12	
MC	1	1	
EC	1	1	
MΦ	0	0	
DCT	4	4	
LH-AL	3	6	
LH-DL	3	3	
IC-B	0	7	
IC-A	8	0	
CD-PC	1	4	
PT-S3	7	6	
PT-S1/S2	6	3	

Figure 3

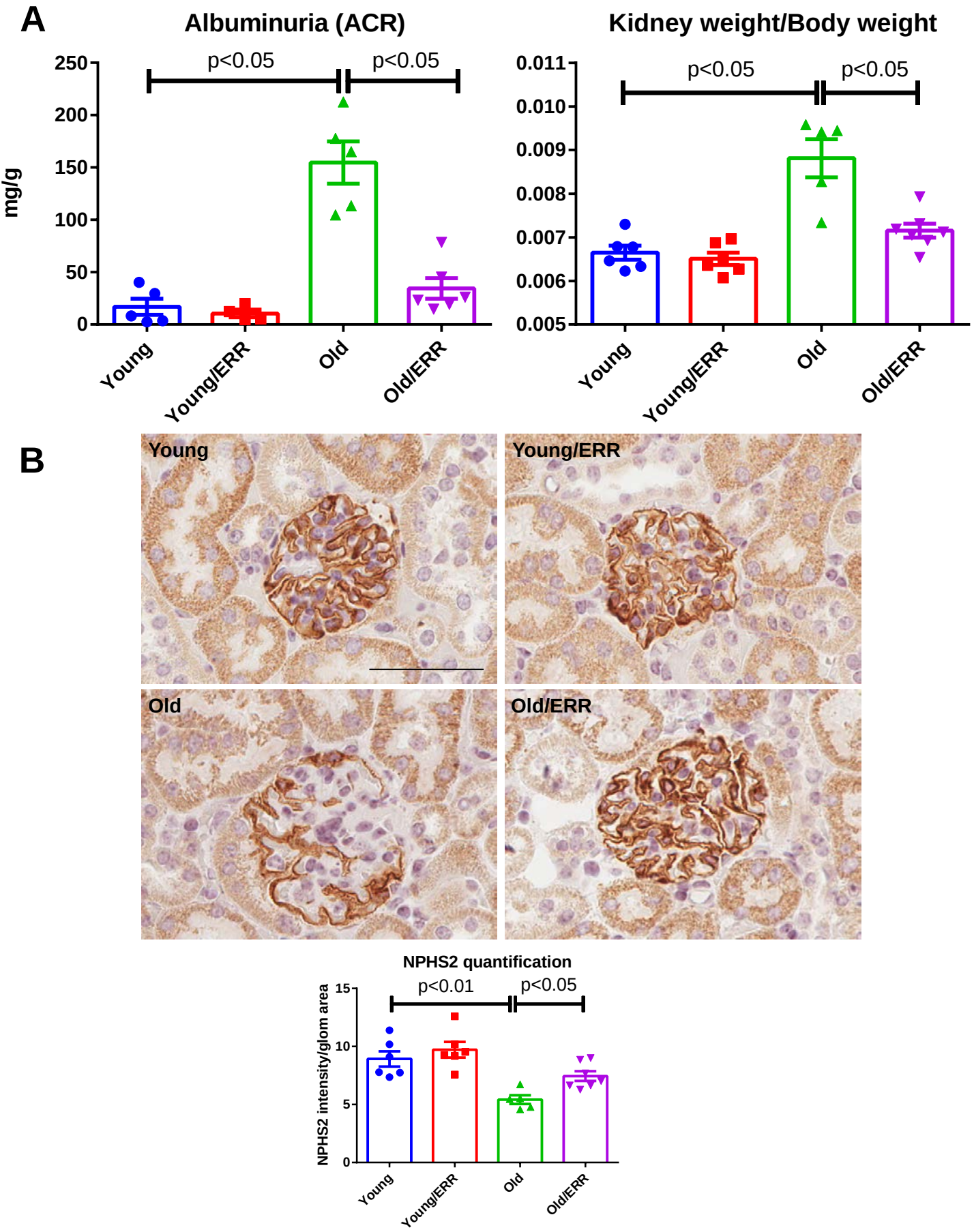
A
Albuminuria (ACR)
mg/g
250
200
150
100
50
0
p<0.05
p<0.05
Young
Young/ERR
Old
Old/ERR
Kidney weight/Body weight
0.011
0.010
0.009
0.008
0.007
0.006
0.005
p<0.05
p<0.05
Young
Young/ERR
Old
Old/ERR
B
Young
Young/ERR
Old
Old/ERR
NPHS2 quantification
NPHS2 intensity/glom area
15
10
5
0
p<0.01
p<0.05
Young
Young/ERR
Old
Old/ERR

Figure 3

C

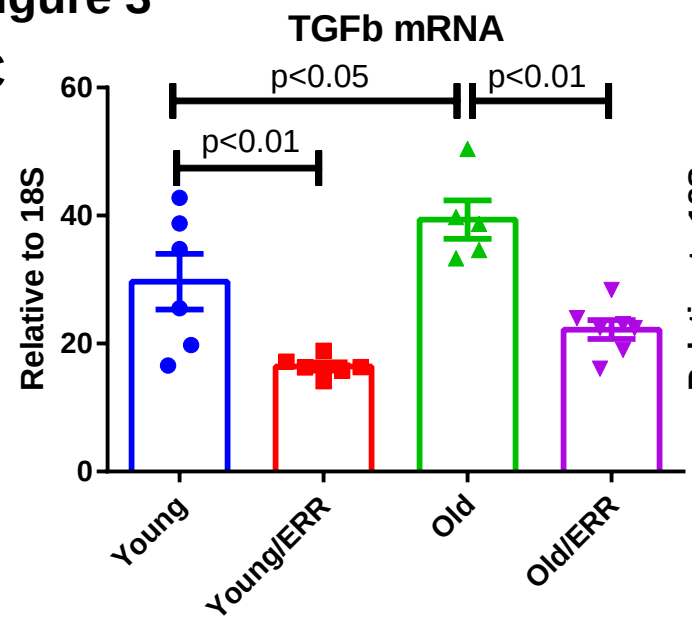
TGFb mRNA
p<0.05
p<0.01
p<0.01
Relative to 18S
60
40
20
0
Young
Young/ERR
Old
Old/ERR

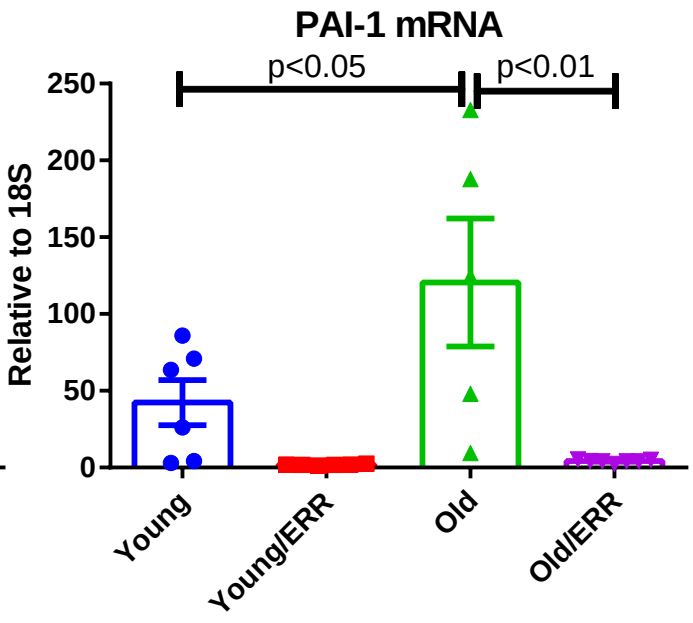
PAI-1 mRNA
p<0.05
p<0.01
Relative to 18S
250
200
150
100
50
0
Young
Young/ERR
Old
Old/ERR

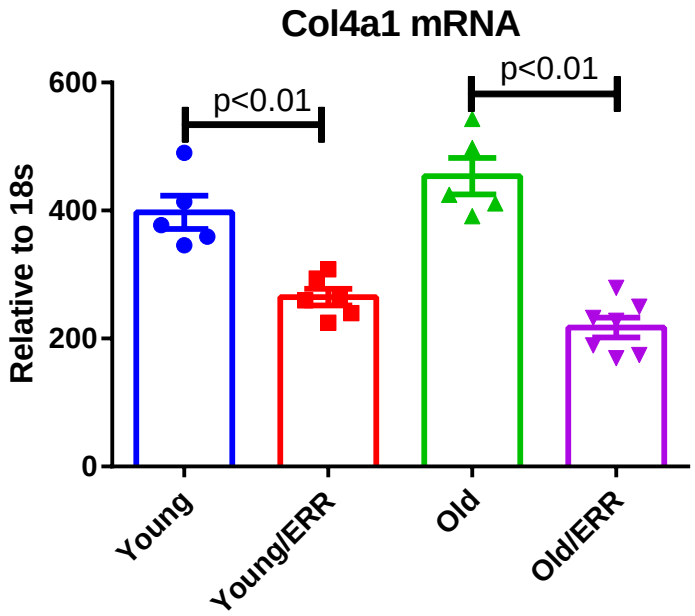
Col4a1 mRNA
p<0.01
p<0.01
Relative to 18s
600
400
200
0
Young
Young/ERR
Old
Old/ERR

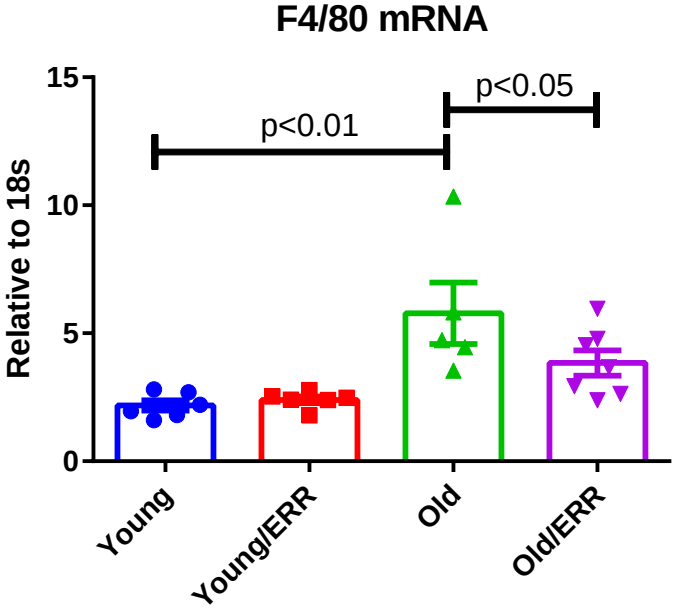
F4/80 mRNA
p<0.01
p<0.05
Relative to 18s
15
10
5
0
Young
Young/ERR
Old
Old/ERR

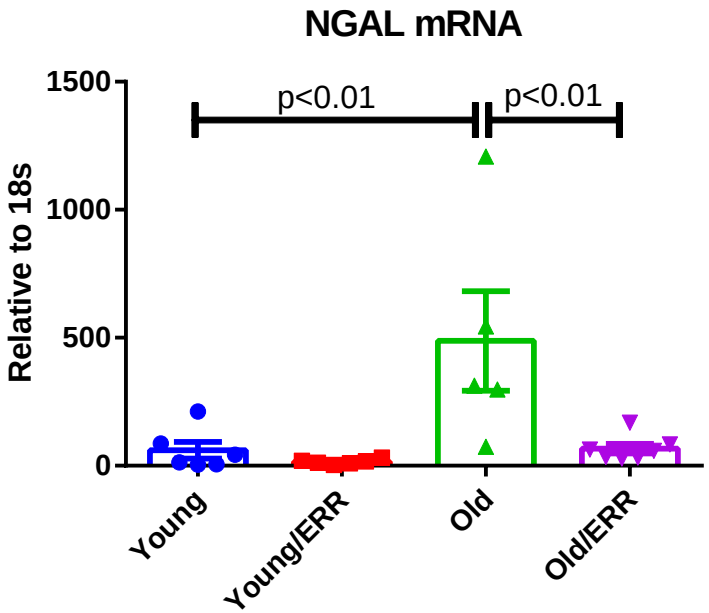
NGAL mRNA
p<0.01
p<0.01
Relative to 18s
1500
1000
500
0
Young
Young/ERR
Old
Old/ERR

Figure 3

D

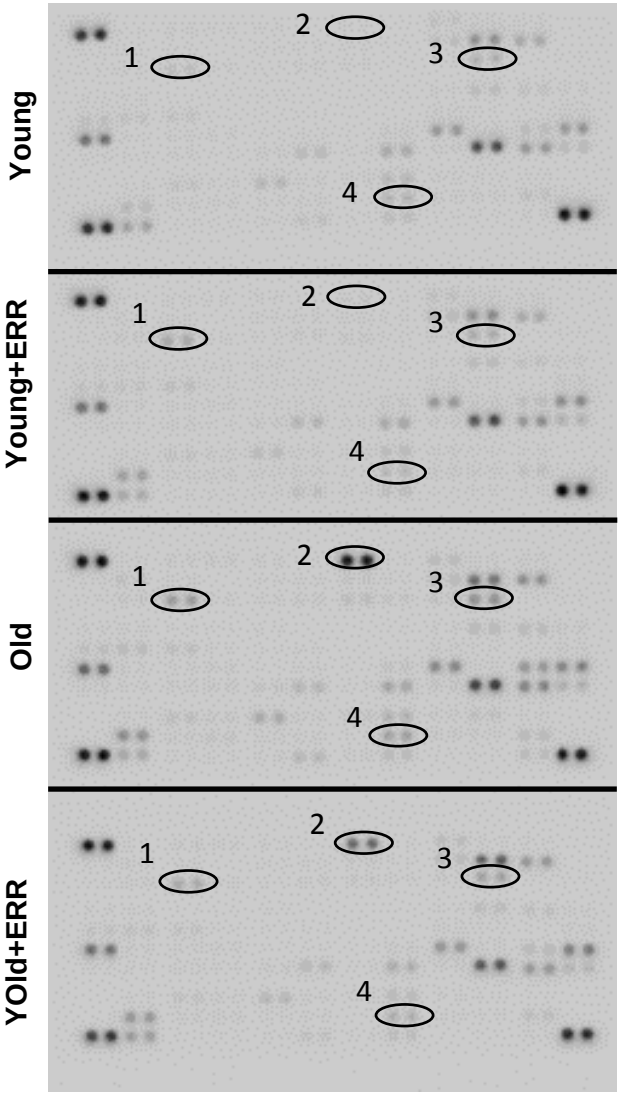
Young
Young+ERR
Old
YOld+ERR
1
2
3
4

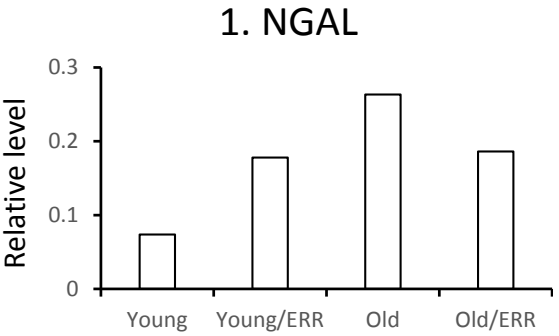
1. NGAL
Relative level
0.3
0.2
0.1
0
Young
Young/ERR
Old
Old/ERR

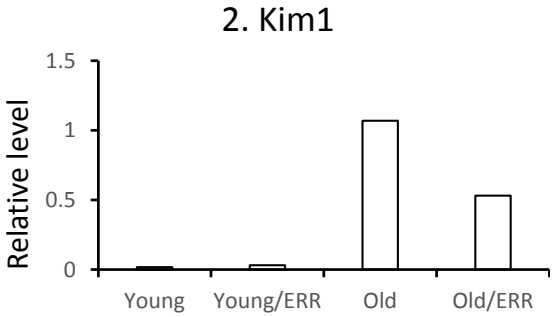
2. Kim1
Relative level
1.5
1
0.5
0
Young
Young/ERR
Old
Old/ERR

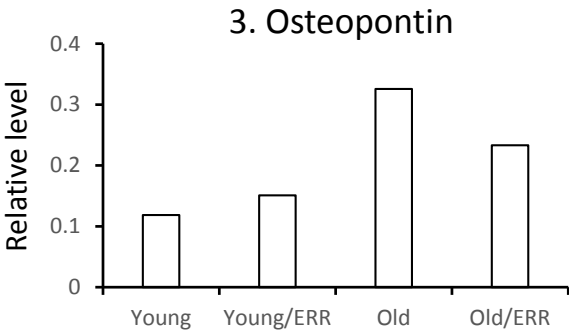
3. Osteopontin
Relative level
0.4
0.3
0.2
0.1
0
Young
Young/ERR
Old
Old/ERR

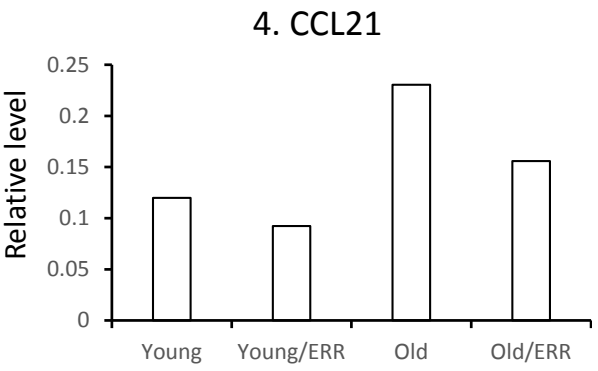
4. CCL21
Relative level
0.25
0.2
0.15
0.1
0.05
0
Young
Young/ERR
Old
Old/ERR

Figure 4

A

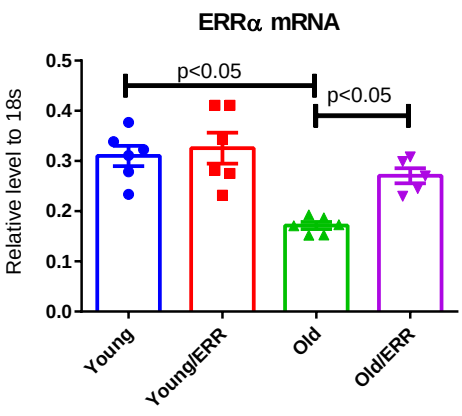
ERRα mRNA
Relative level to 18s
0.5
0.4
0.3
0.2
0.1
0.0
p<0.05
p<0.05
Young
Young/ERR
Old
Old/ERR

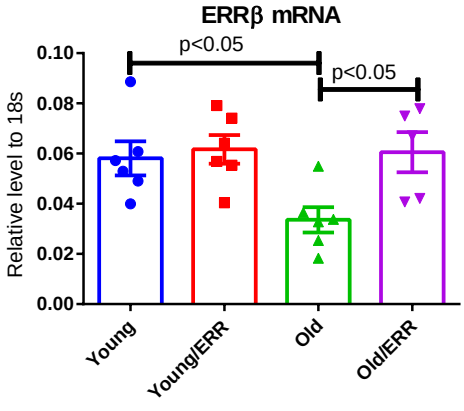
ERRβ mRNA
Relative level to 18s
0.10
0.08
0.06
0.04
0.02
0.00
p<0.05
p<0.05
Young
Young/ERR
Old
Old/ERR

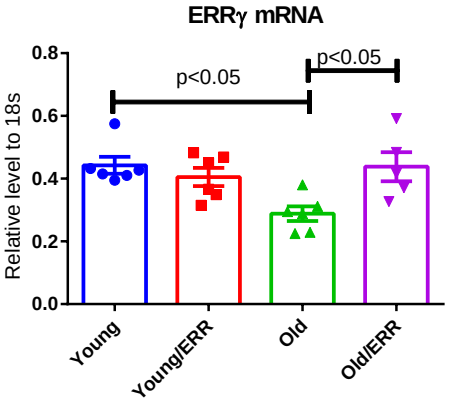
ERRγ mRNA
Relative level to 18s
0.8
0.6
0.4
0.2
0.0
p<0.05
p<0.05
Young
Young/ERR
Old
Old/ERR

Figure 4

B

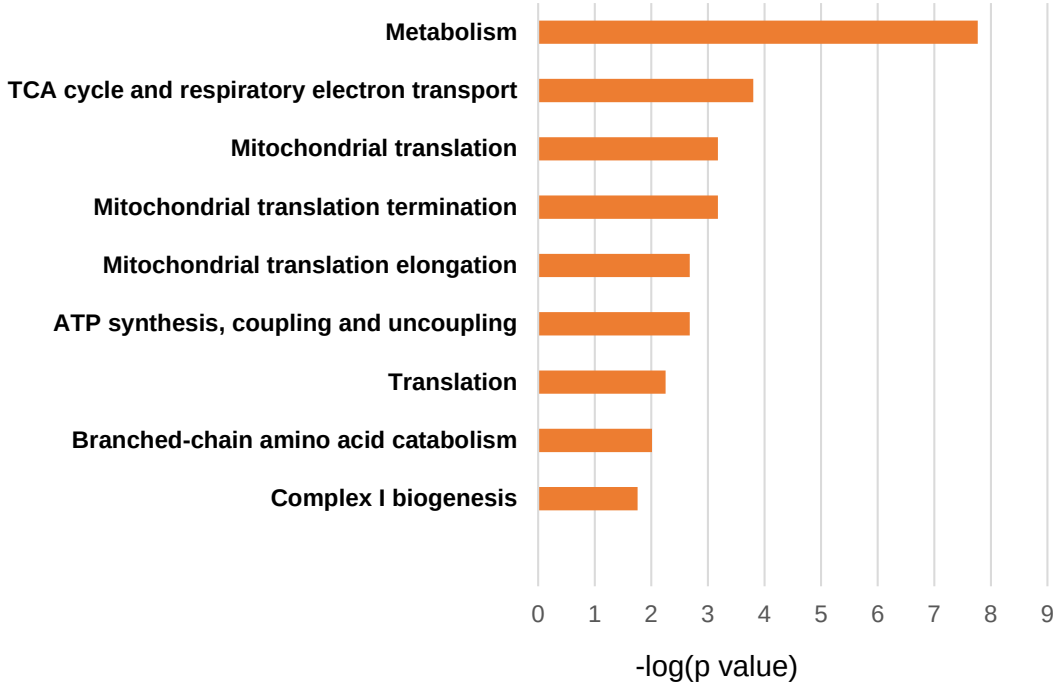
Metabolism
TCA cycle and respiratory electron transport
Mitochondrial translation
Mitochondrial translation termination
Mitochondrial translation elongation
ATP synthesis, coupling and uncoupling
Translation
Branched-chain amino acid catabolism
Complex I biogenesis
0
1
2
3
4
5
6
7
8
9
-log(p value)

C

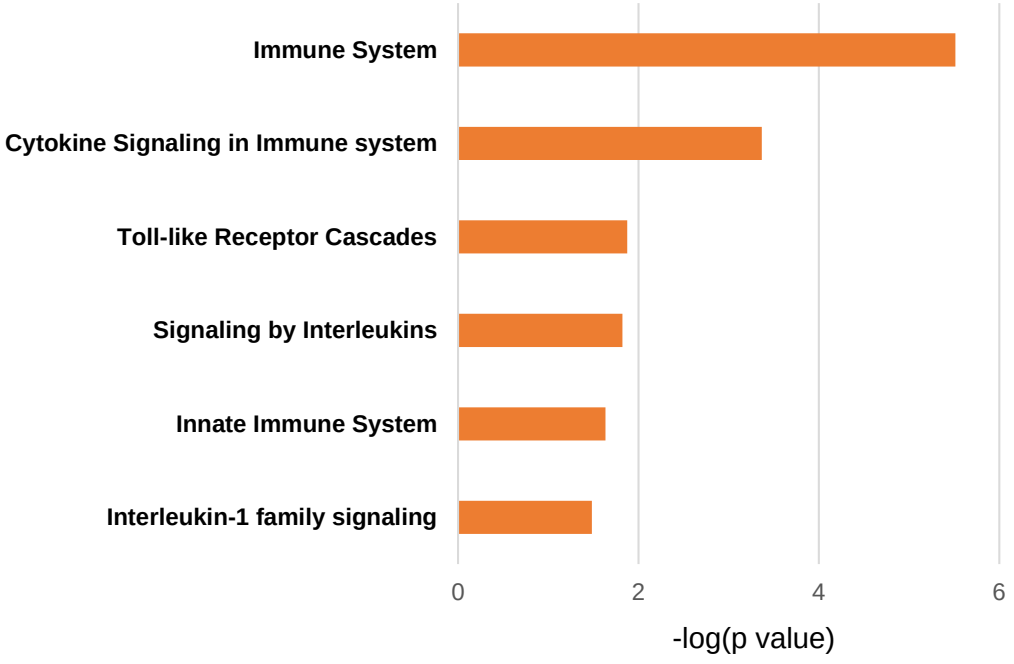
Immune System
Cytokine Signaling in Immune system
Toll-like Receptor Cascades
Signaling by Interleukins
Innate Immune System
Interleukin-1 family signaling
0
2
4
6
-log(p value)

Figure 3

D

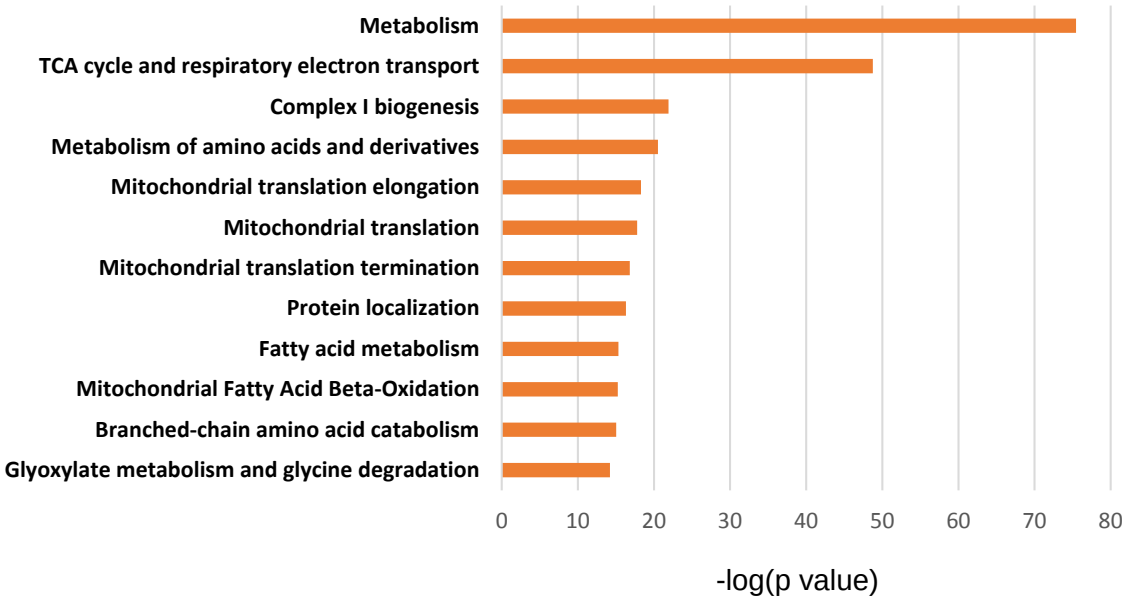
Metabolism
TCA cycle and respiratory electron transport
Complex I biogenesis
Metabolism of amino acids and derivatives
Mitochondrial translation elongation
Mitochondrial translation
Mitochondrial translation termination
Protein localization
Fatty acid metabolism
Mitochondrial Fatty Acid Beta-Oxidation
Branched-chain amino acid catabolism
Glyoxylate metabolism and glycine degradation
0
10
20
30
40
50
60
70
80
-log(p value)

E

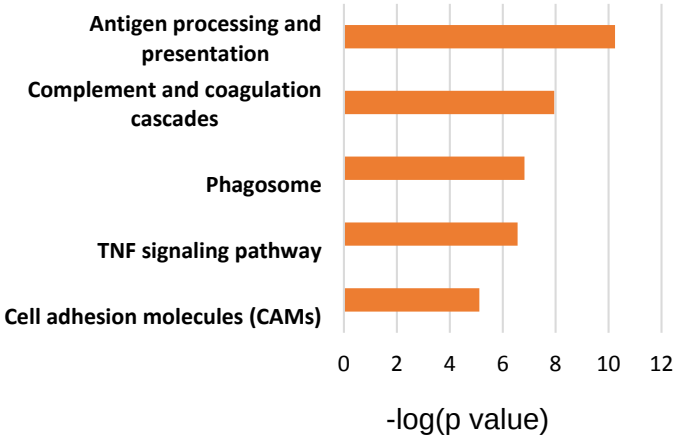
Antigen processing and presentation
Complement and coagulation cascades
Phagosome
TNF signaling pathway
Cell adhesion molecules (CAMs)
0
2
4
6
8
10
12
-log(p value)

F

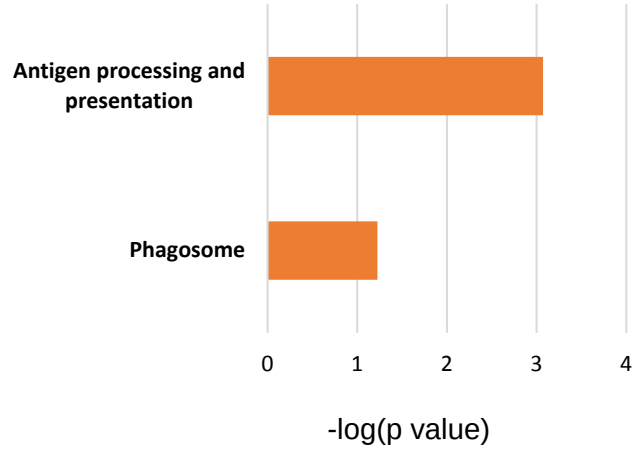
Antigen processing and presentation
Phagosome
0
1
2
3
4
-log(p value)

Figure 5

A

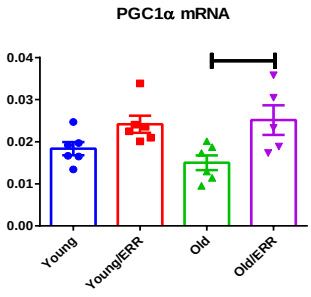
PGC1α mRNA
0.04
0.03
0.02
0.01
0.00
Young
Young/ERR
Old
Old/ERR

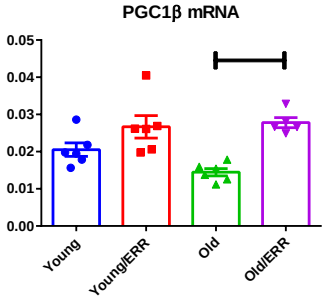
PGC1β mRNA
0.05
0.04
0.03
0.02
0.01
0.00
Young
Young/ERR
Old
Old/ERR

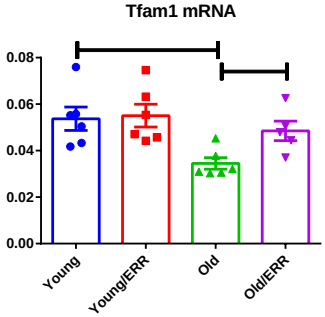
Tfam1 mRNA
0.08
0.06
0.04
0.02
0.00
Young
Young/ERR
Old
Old/ERR

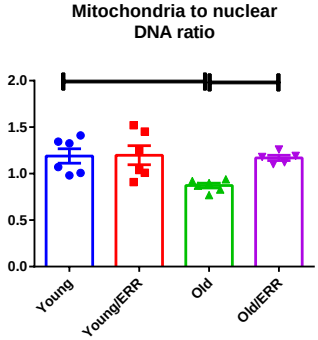
Mitochondria to nuclear DNA ratio
2.0
1.5
1.0
0.5
0.0
Young
Young/ERR
Old
Old/ERR

Figure 5

B

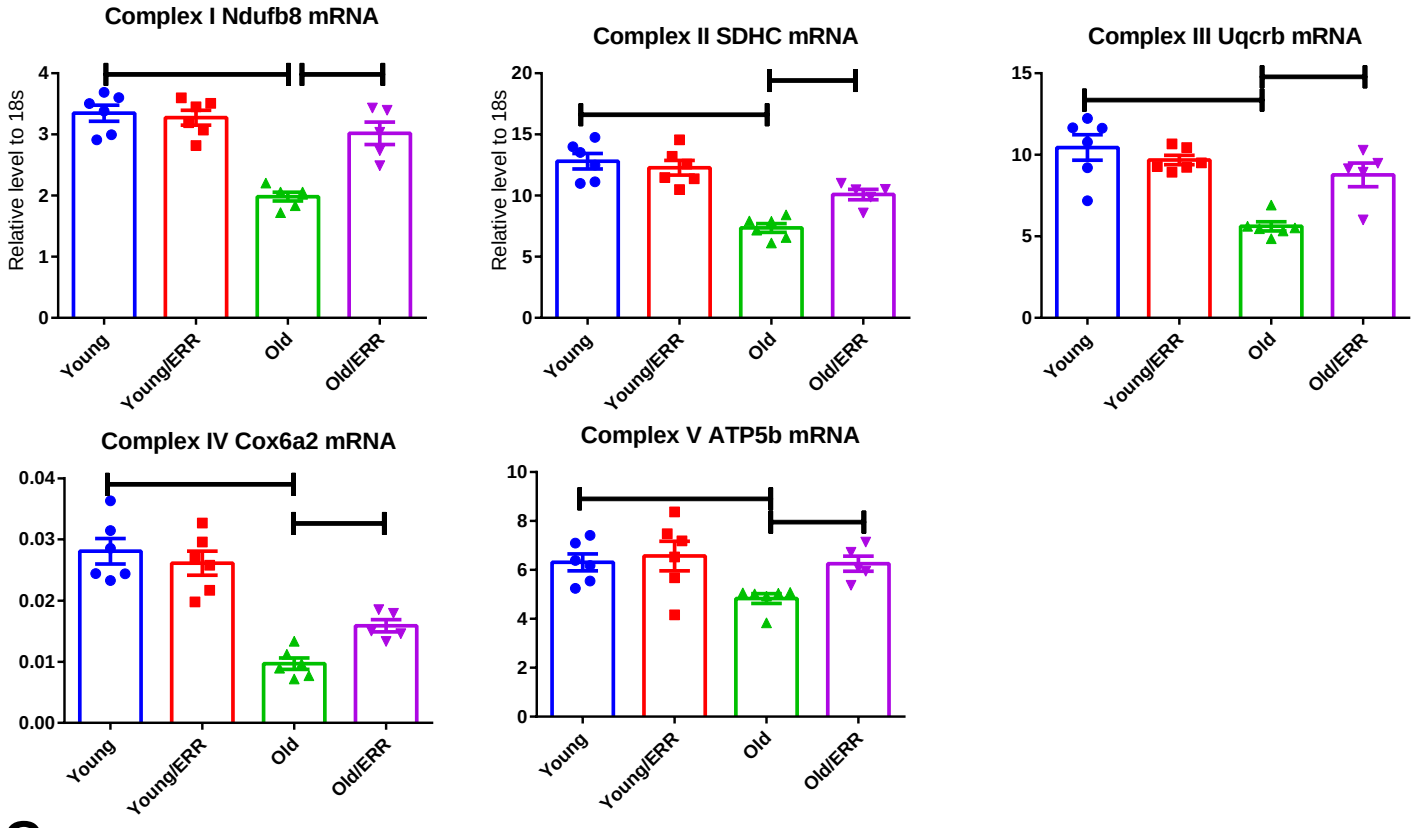
Complex I Ndufb8 mRNA
Relative level to 18s
Young
Young/ERR
Old
Old/ERR
Complex II SDHC mRNA
Complex III Uqcrb mRNA
Complex IV Cox6a2 mRNA
Complex V ATP5b mRNA

C

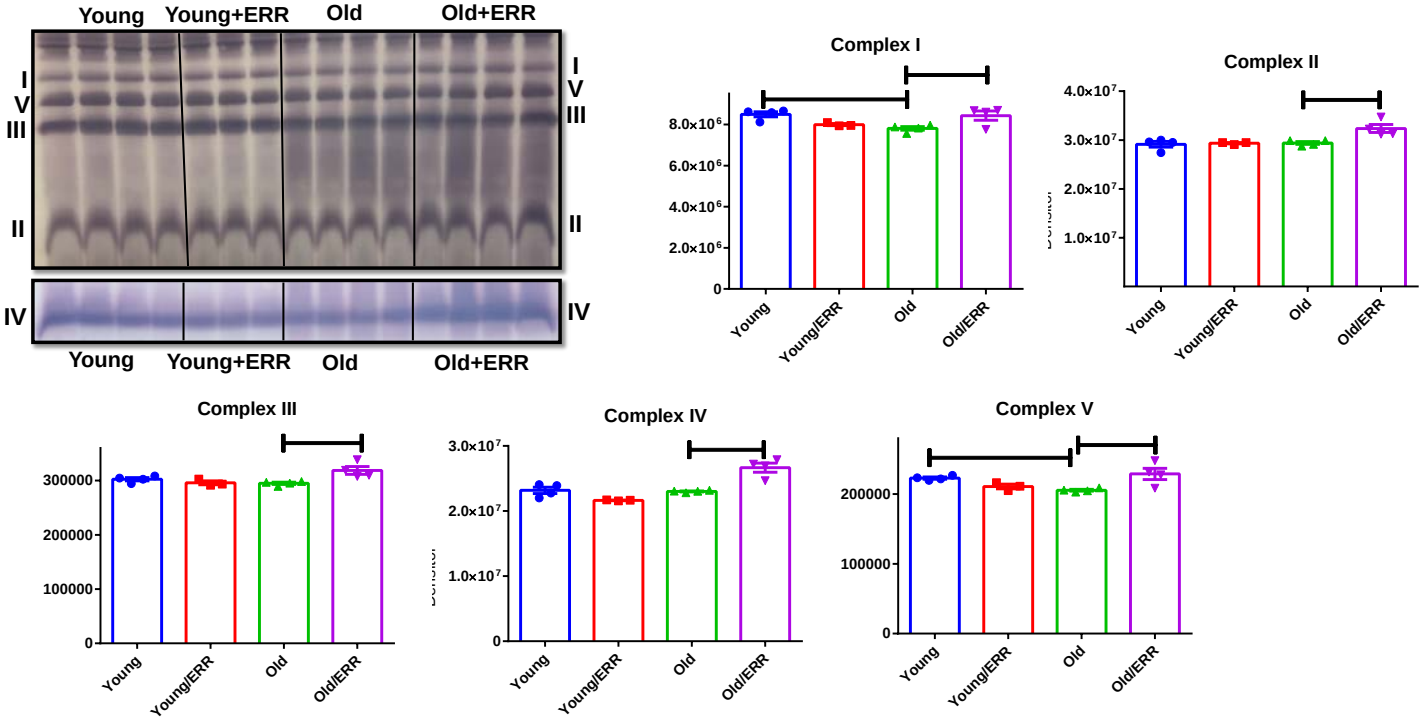
Young
Young+ERR
Old
Old+ERR
I
V
III
II
IV
Complex I
Complex II
Complex III
Complex IV
Complex V

Figure 5

D

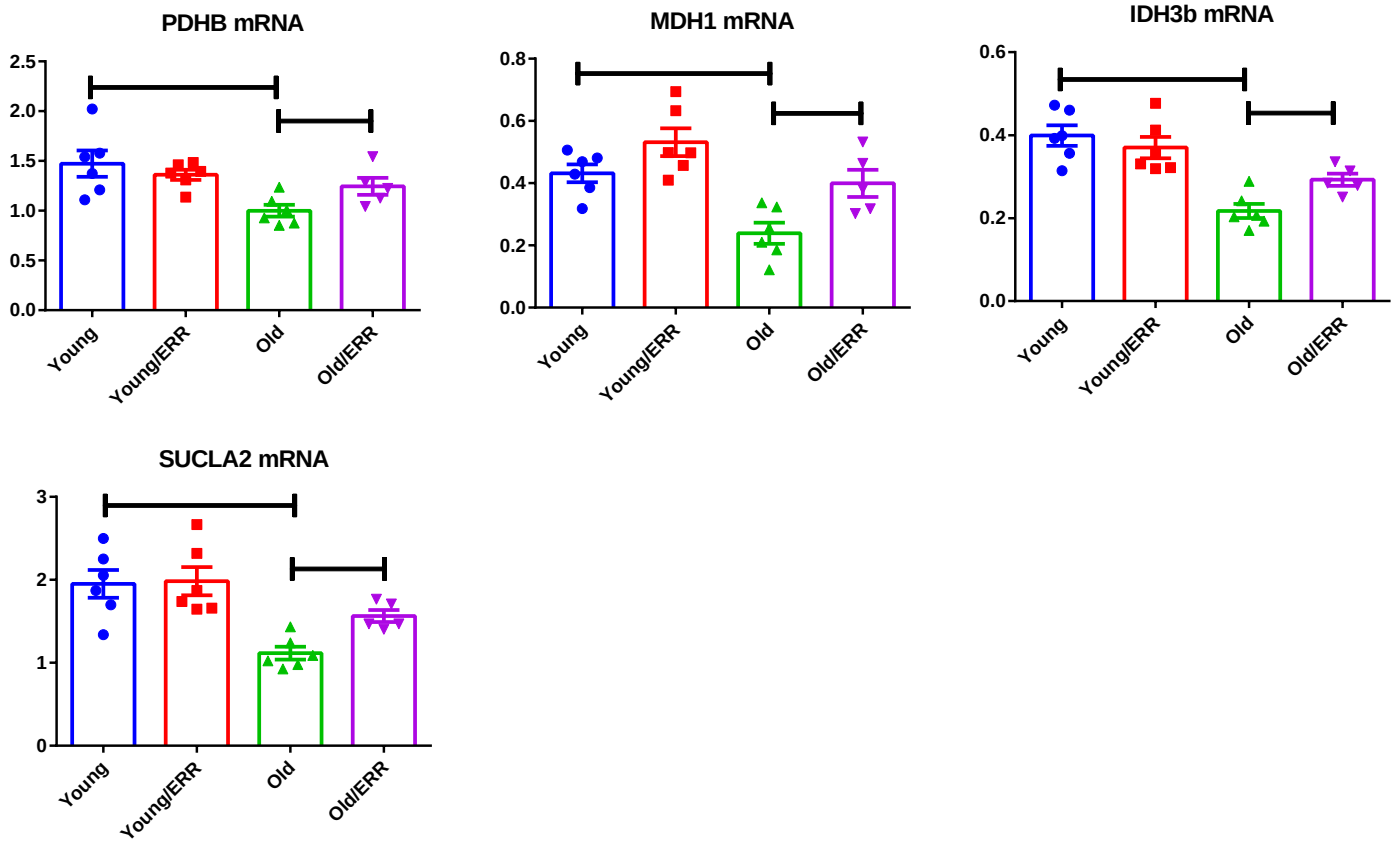
PDHB mRNA
2.5
2.0
1.5
1.0
0.5
0.0
Young
Young/ERR
Old
Old/ERR
MDH1 mRNA
0.8
0.6
0.4
0.2
0.0
Young
Young/ERR
Old
Old/ERR
IDH3b mRNA
0.6
0.4
0.2
0.0
Young
Young/ERR
Old
Old/ERR
SUCLA2 mRNA
3
2
1
0
Young
Young/ERR
Old
Old/ERR

E

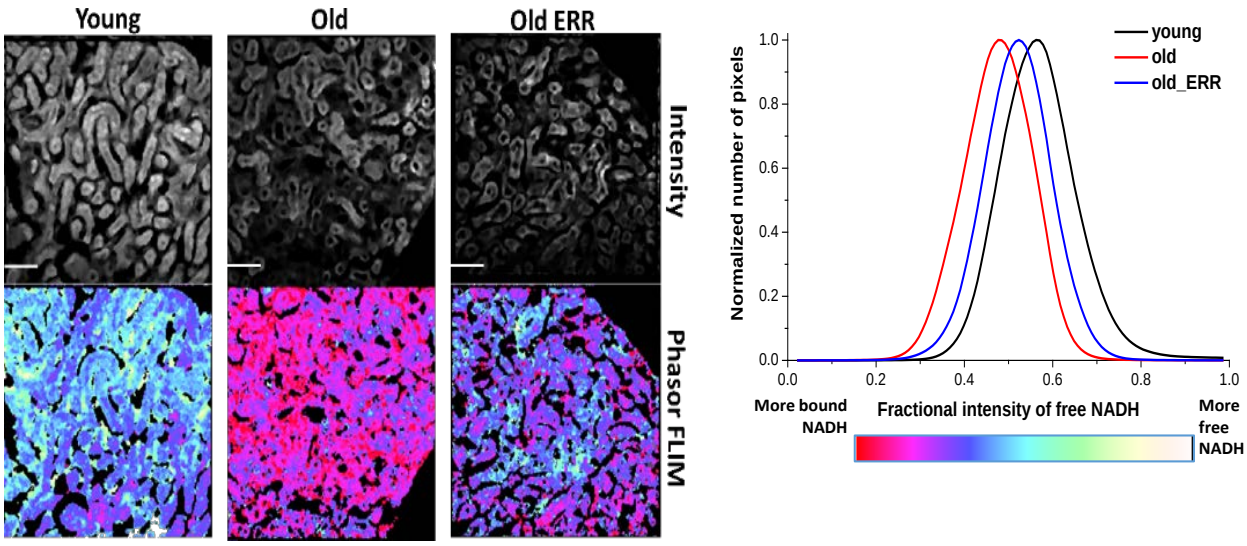
Young
Old
Old ERR
Intensity
Phasor FLIM
young
old
old_ERR
Normalized number of pixels
1.0
0.8
0.6
0.4
0.2
0.0
0.0
0.2
0.4
0.6
0.8
1.0
More bound NADH
Fractional intensity of free NADH
More free NADH

Figure 5

F

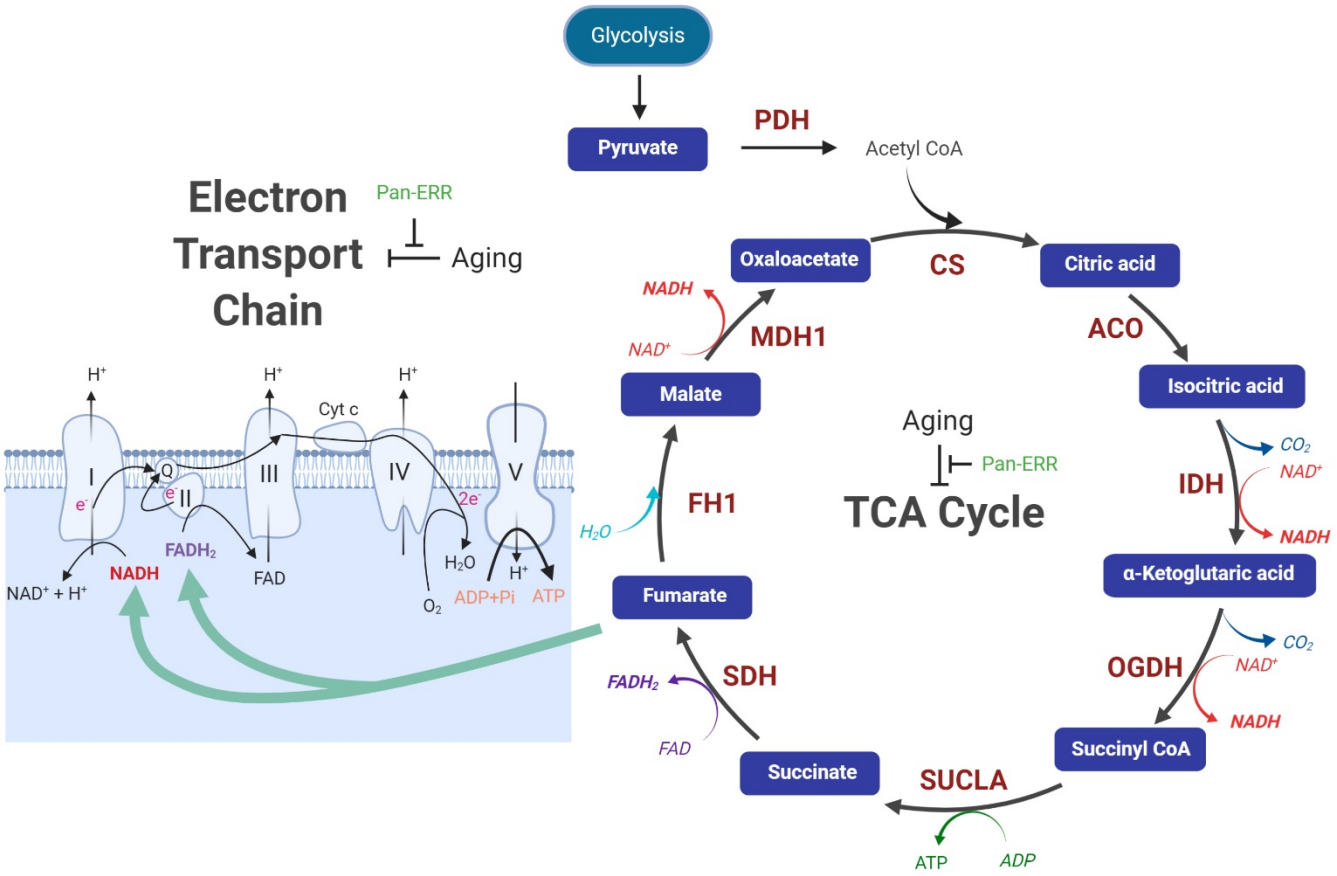
Glycolysis
Pyruvate
PDH
Acetyl CoA
Electron Transport Chain
Pan-ERR
Aging
Oxaloacetate
CS
Citric acid
NADH
NAD+
MDH1
ACO
Malate
Isocitric acid
Aging
Pan-ERR
TCA Cycle
IDH
CO2
NAD+
NADH
H2O
FH1
α-Ketoglutaric acid
Fumarate
OGDH
CO2
NAD+
NADH
FADH2
SDH
FAD
Succinyl CoA
Succinate
SUCLA
ATP
ADP
H+
Cyt c
I
II
III
IV
V
Q
e-
2e-
FADH2
NADH
FAD
NAD+ + H+
H2O
O2
ADP+Pi
ATP

G

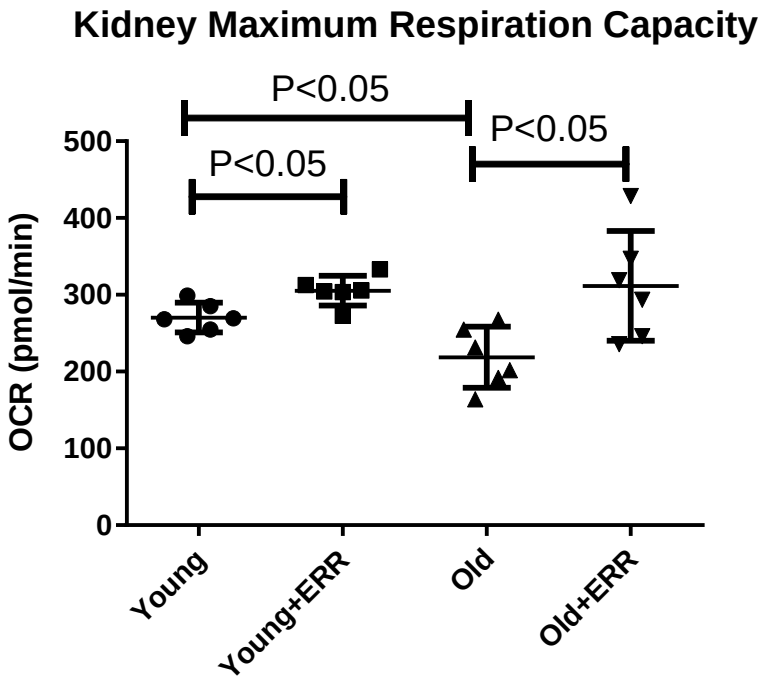
Kidney Maximum Respiration Capacity
P<0.05
P<0.05
P<0.05
OCR (pmol/min)
500
400
300
200
100
0
Young
Young+ERR
Old
Old+ERR

Figure 5

H

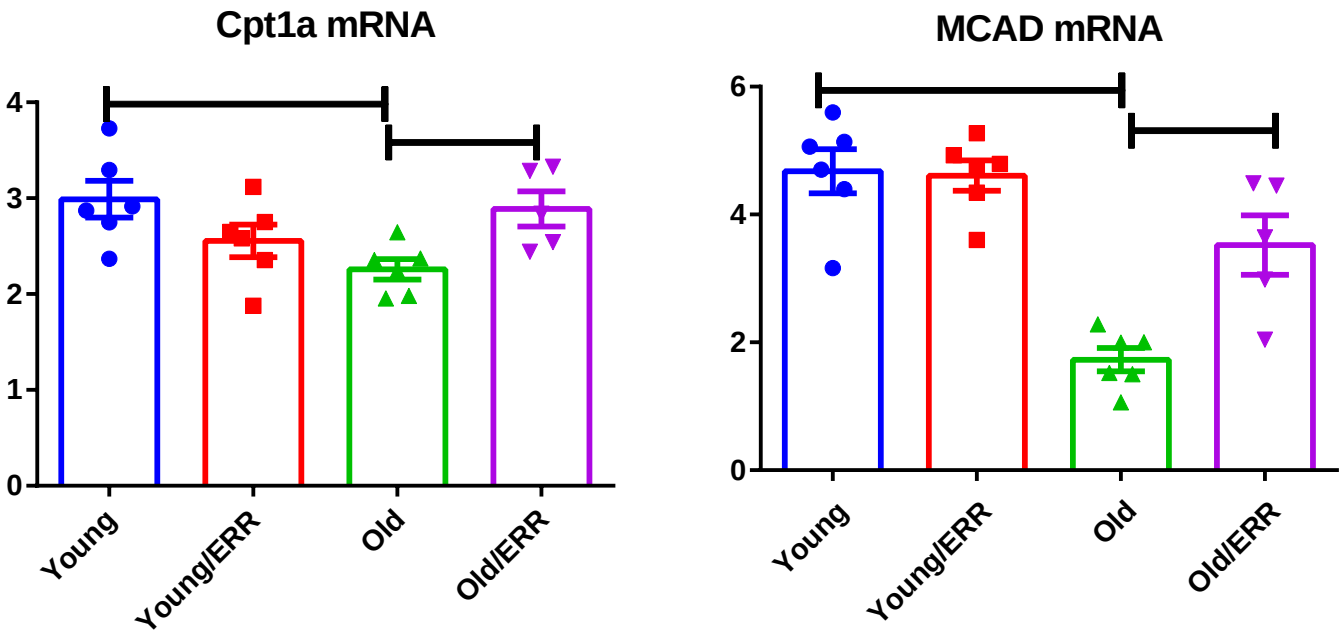
Cpt1a mRNA
4
3
2
1
0
Young
Young/ERR
Old
Old/ERR
MCAD mRNA
6
4
2
0
Young
Young/ERR
Old
Old/ERR

Figure 5

I

Young

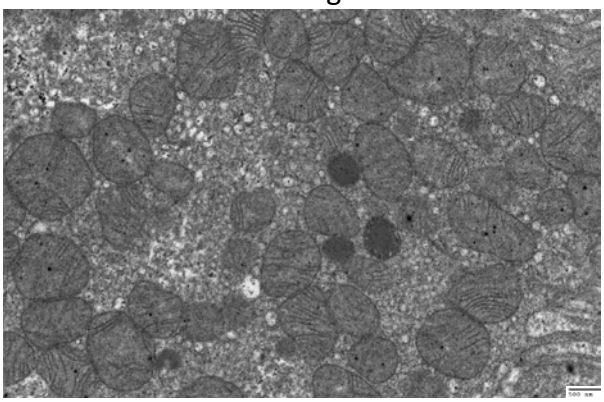

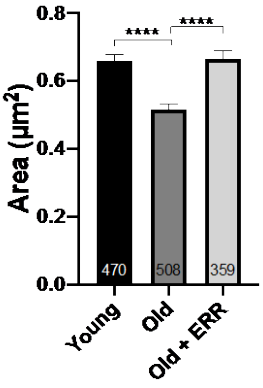

Old

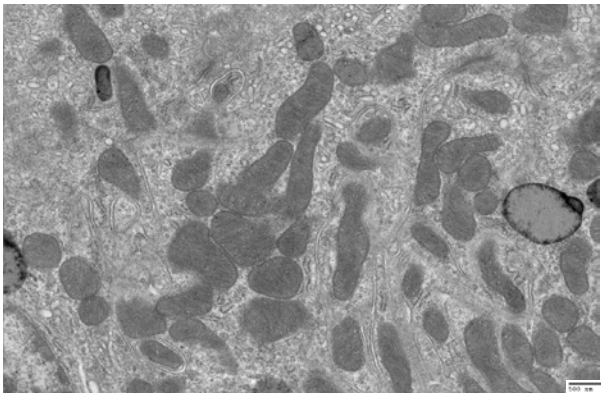

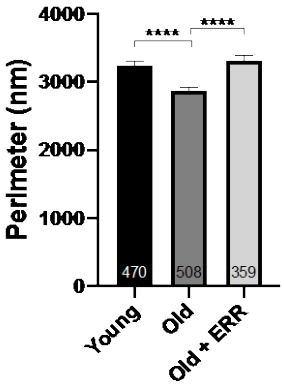

Old + ERR

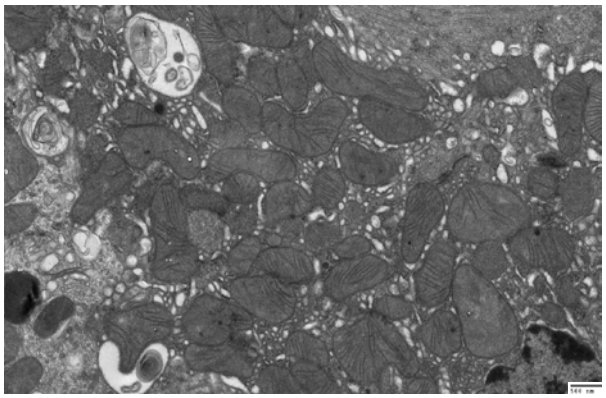

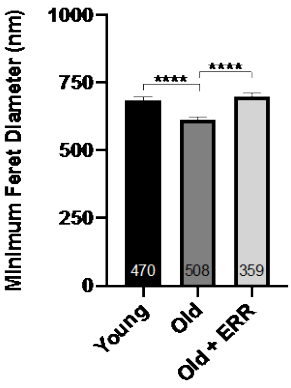

Figure 5

J

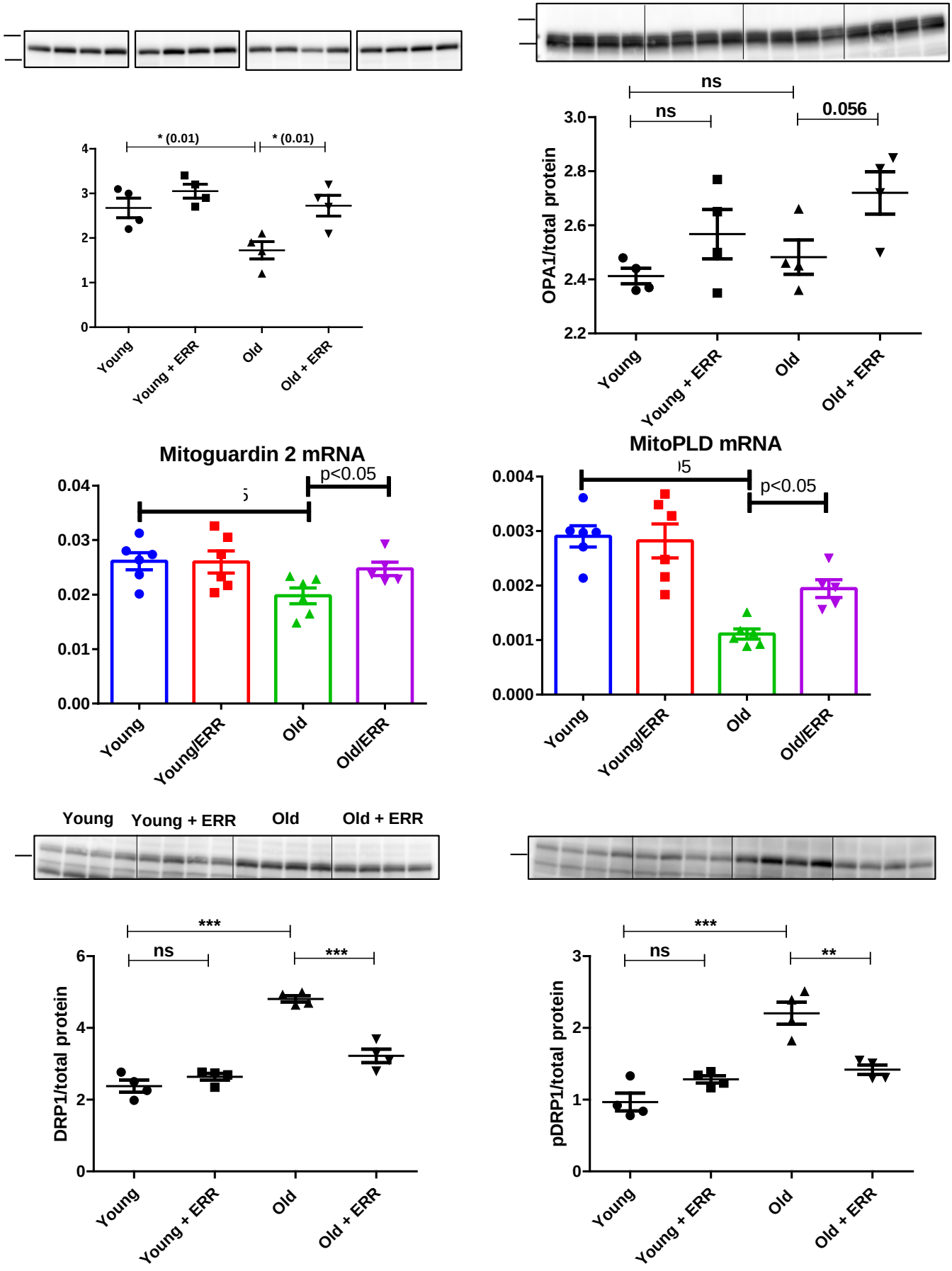
* (0.01)
* (0.01)
Young
Young + ERR
Old
Old + ERR
ns
ns
0.056
OPA1/total protein
Mitoguardin 2 mRNA
p<0.05
Young
Young/ERR
Old
Old/ERR
MitoPLD mRNA
p<0.05
Young
Young + ERR
Old
Old + ERR
***
ns
***
DRP1/total protein
***
ns
**
pDRP1/total protein

Figure 6

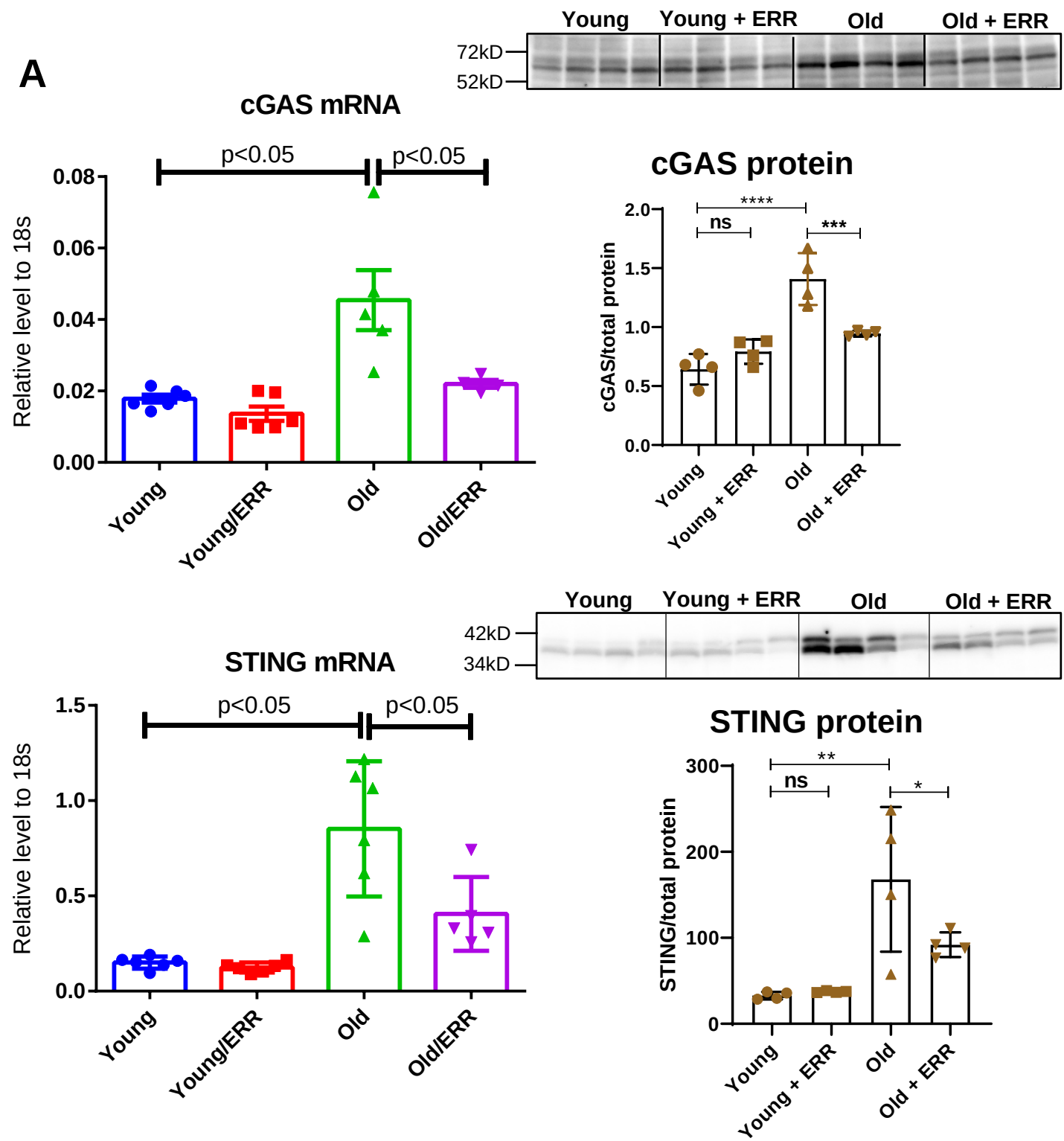
A
Young
Young + ERR
Old
Old + ERR
72kD
52kD
cGAS mRNA
p<0.05
p<0.05
Relative level to 18s
0.08
0.06
0.04
0.02
0.00
Young
Young/ERR
Old
Old/ERR
cGAS protein
****
ns
***
cGAS/total protein
2.0
1.5
1.0
0.5
0.0
Young
Young + ERR
Old
Old + ERR
Young
Young + ERR
Old
Old + ERR
42kD
34kD
STING mRNA
p<0.05
p<0.05
Relative level to 18s
1.5
1.0
0.5
0.0
Young
Young/ERR
Old
Old/ERR
STING protein
**
ns
*
STING/total protein
300
200
100
0
Young
Young + ERR
Old
Old + ERR

Figure 6

B

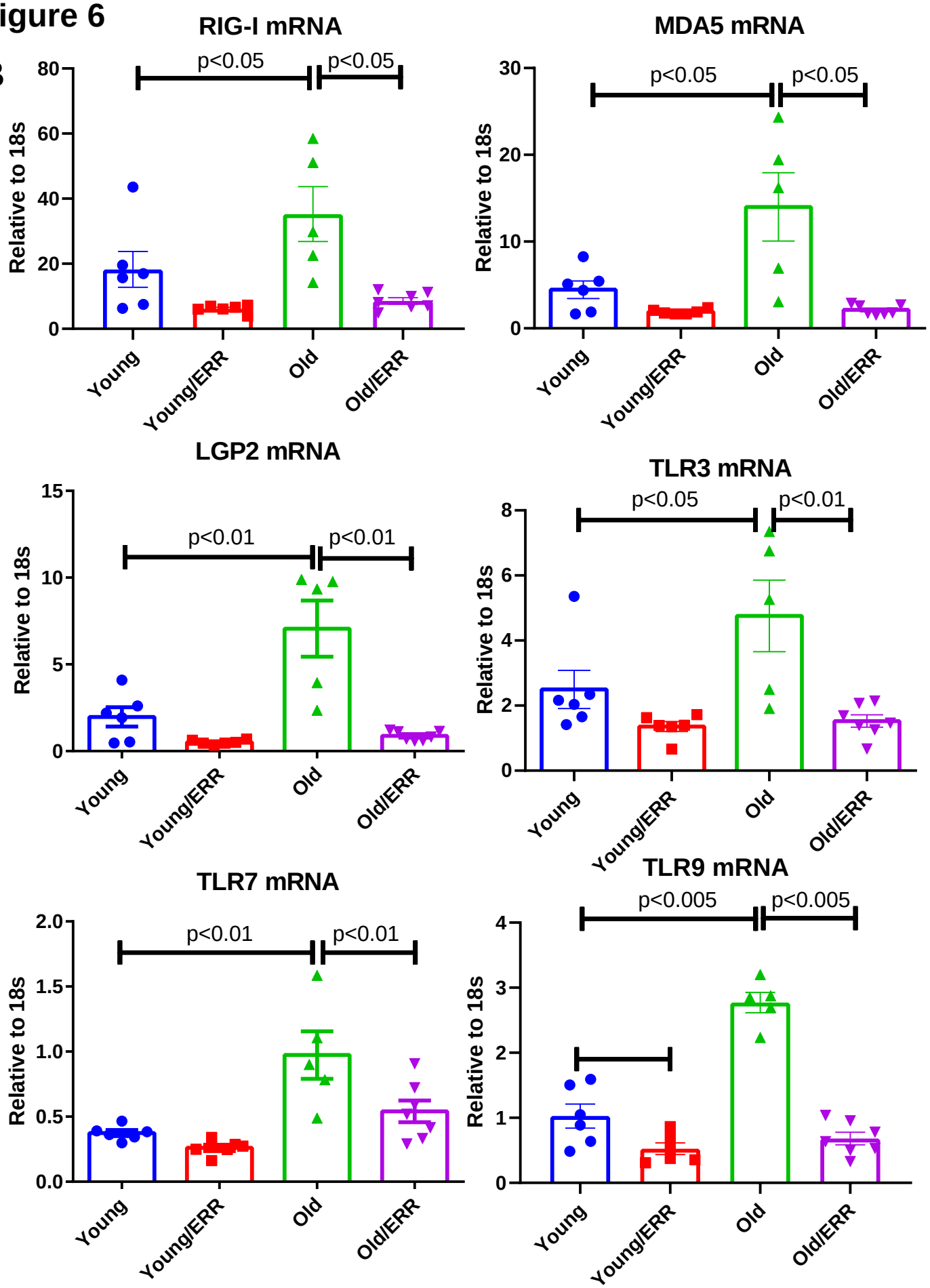
RIG-I mRNA
p<0.05
p<0.05
Relative to 18s
80
60
40
20
0
Young
Young/ERR
Old
Old/ERR
MDA5 mRNA
p<0.05
p<0.05
Relative to 18s
30
20
10
0
Young
Young/ERR
Old
Old/ERR
LGP2 mRNA
p<0.01
p<0.01
Relative to 18s
15
10
5
0
Young
Young/ERR
Old
Old/ERR
TLR3 mRNA
p<0.05
p<0.01
Relative to 18s
8
6
4
2
0
Young
Young/ERR
Old
Old/ERR
TLR7 mRNA
p<0.01
p<0.01
Relative to 18s
2.0
1.5
1.0
0.5
0.0
Young
Young/ERR
Old
Old/ERR
TLR9 mRNA
p<0.005
p<0.005
Relative to 18s
4
3
2
1
0
Young
Young/ERR
Old
Old/ERR

Figure 6

C

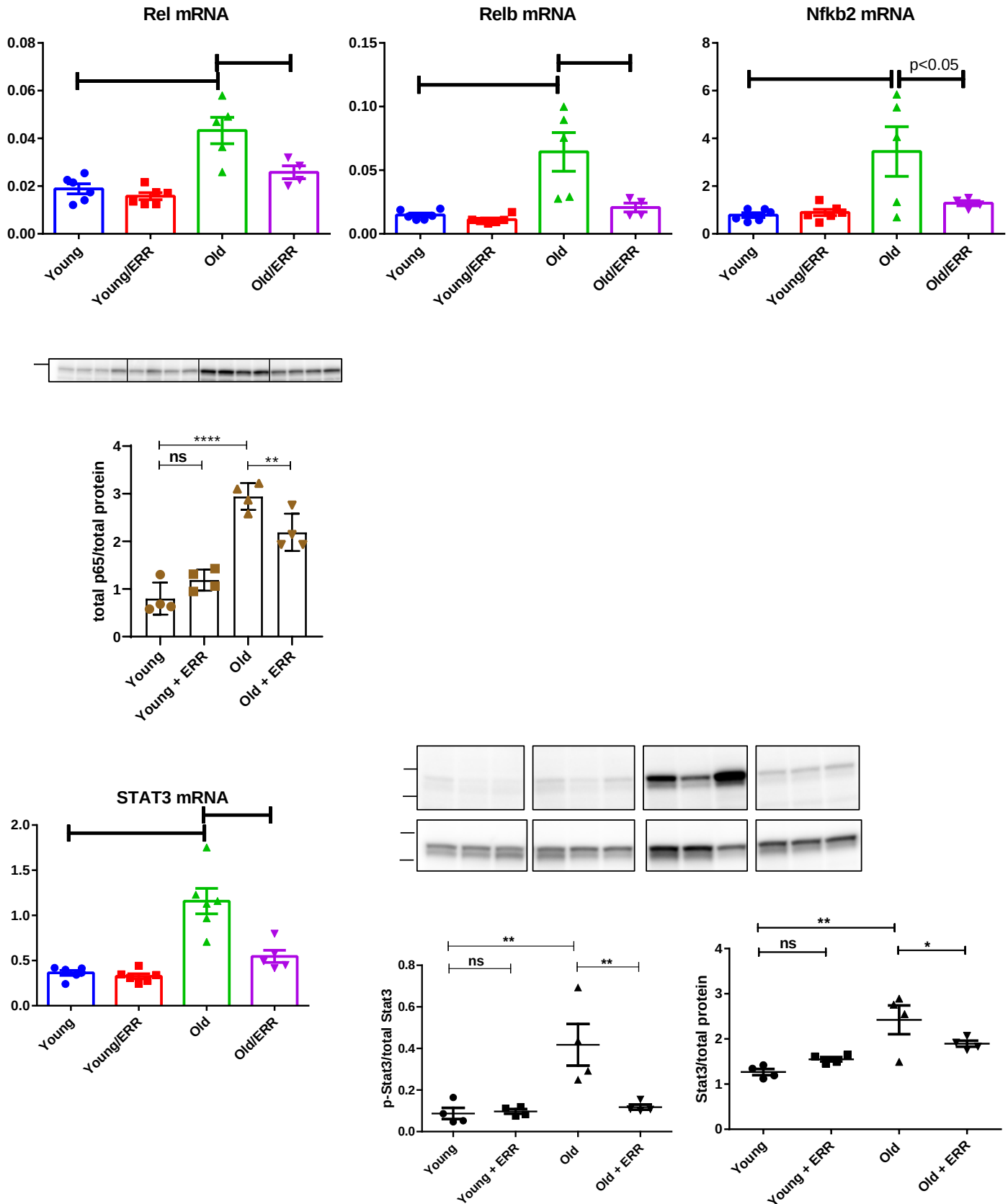
Rel mRNA
Relb mRNA
Nfkb2 mRNA
p<0.05
Young
Young/ERR
Old
Old/ERR
total p65/total protein
****
ns
**
Young + ERR
Old + ERR
STAT3 mRNA
p-Stat3/total Stat3
Stat3/total protein
*

Figure 6

D

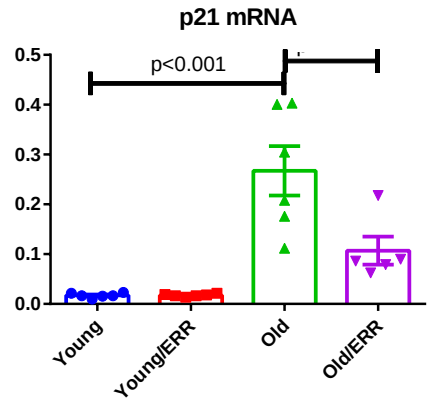
p21 mRNA
p<0.001
0.5
0.4
0.3
0.2
0.1
0.0
Young
Young/ERR
Old
Old/ERR

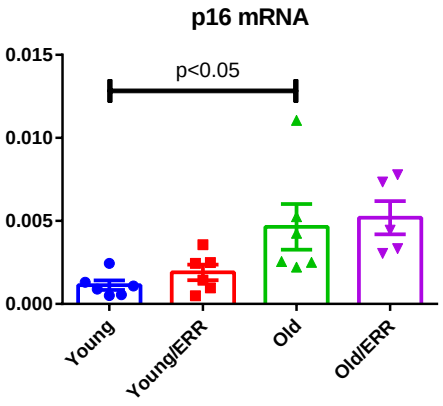
p16 mRNA
p<0.05
0.015
0.010
0.005
0.000
Young
Young/ERR
Old
Old/ERR

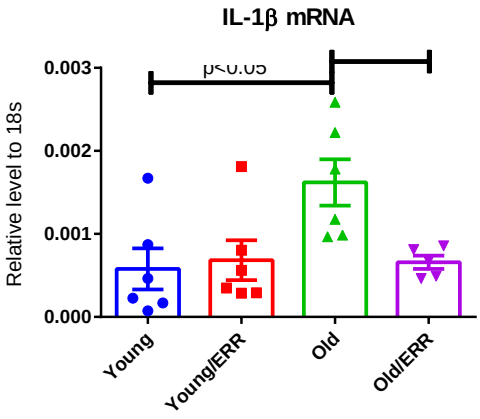
IL-1β mRNA
p<0.05
Relative level to 18s
0.003
0.002
0.001
0.000
Young
Young/ERR
Old
Old/ERR

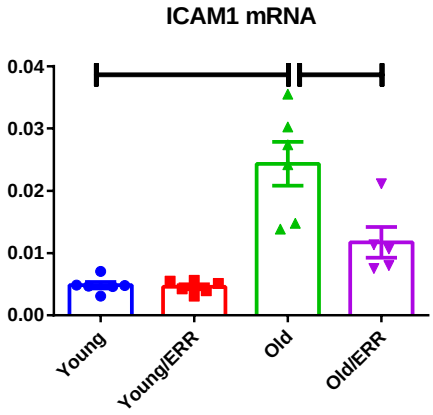
ICAM1 mRNA
0.04
0.03
0.02
0.01
0.00
Young
Young/ERR
Old
Old/ERR

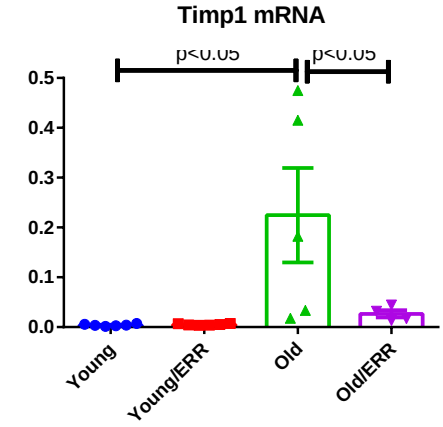
Timp1 mRNA
p<0.05
p<0.05
0.5
0.4
0.3
0.2
0.1
0.0
Young
Young/ERR
Old
Old/ERR

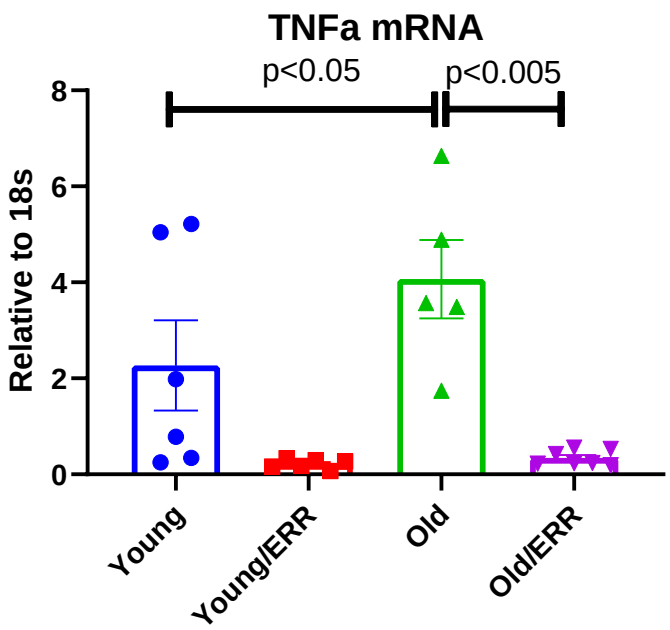
TNFa mRNA
p<0.05
p<0.005
Relative to 18s
8
6
4
2
0
Young
Young/ERR
Old
Old/ERR

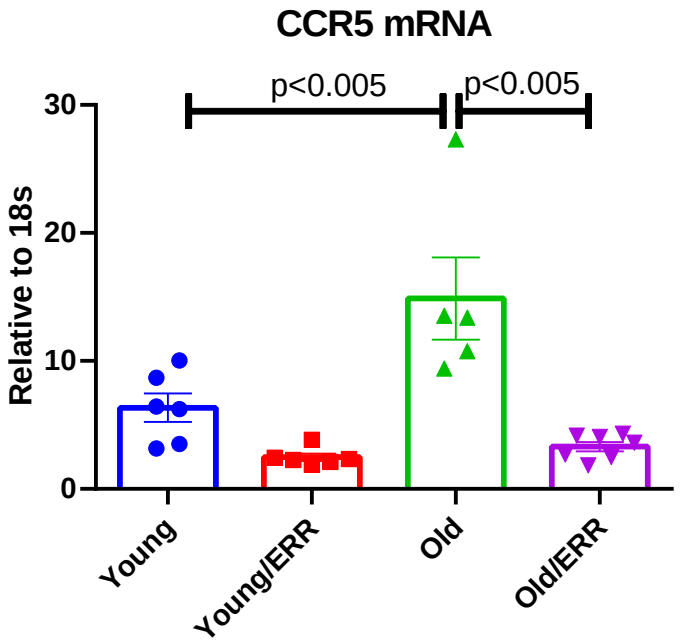
CCR5 mRNA
p<0.005
p<0.005
Relative to 18s
30
20
10
0
Young
Young/ERR
Old
Old/ERR

Figure 7

A

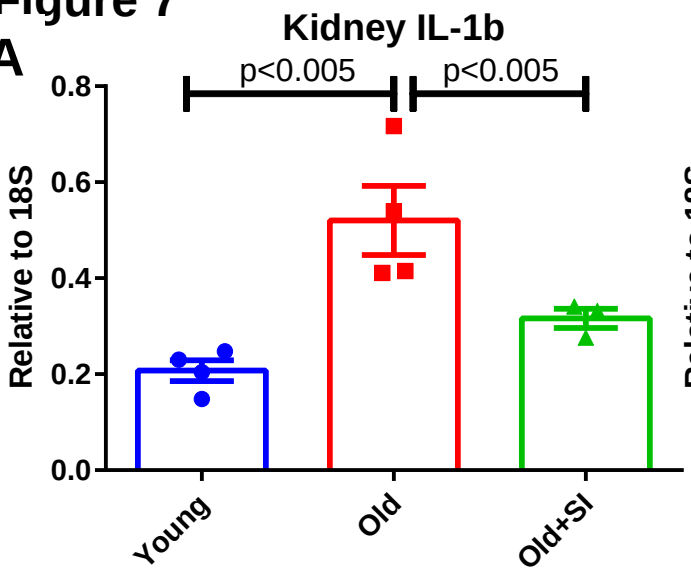
Kidney IL-1b
p<0.005
p<0.005
Relative to 18S
0.8
0.6
0.4
0.2
0.0
Young
Old
Old+SI

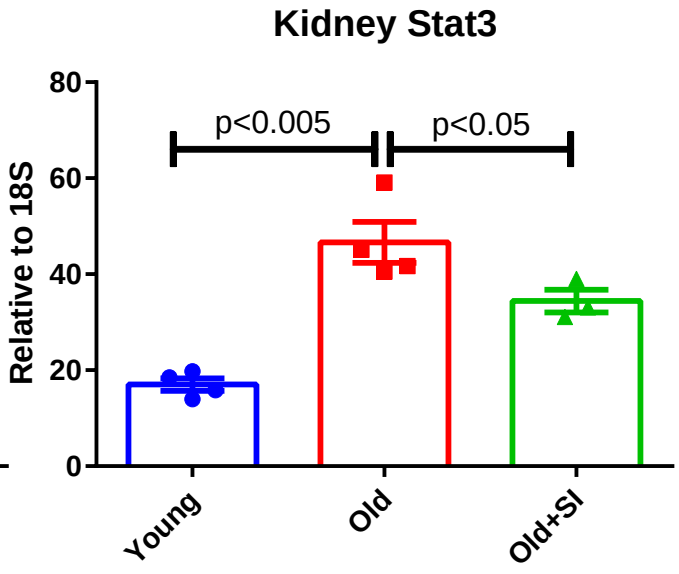
Kidney Stat3
p<0.005
p<0.05
Relative to 18S
80
60
40
20
0
Young
Old
Old+SI

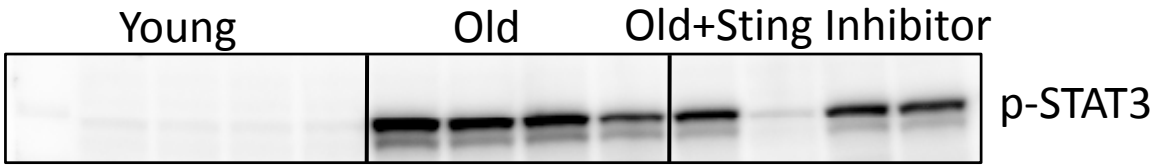
Young
Old
Old+Sting Inhibitor
p-STAT3

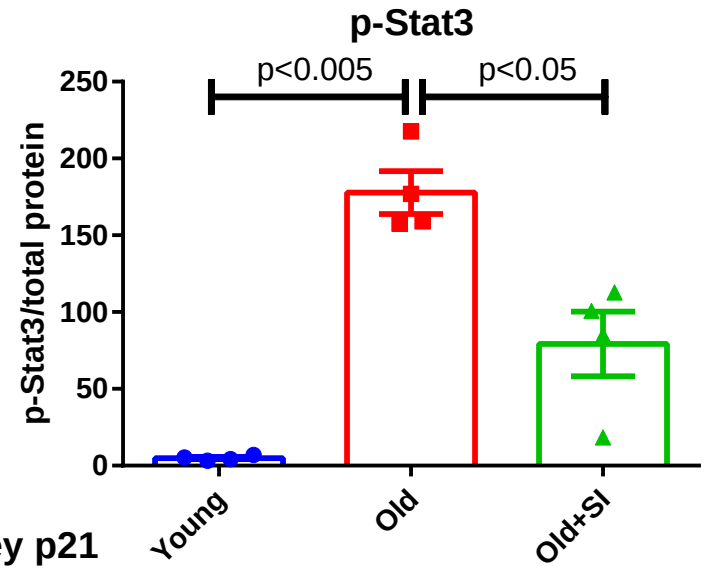
p-Stat3
p<0.005
p<0.05
p-Stat3/total protein
250
200
150
100
50
0
Young
Old
Old+SI

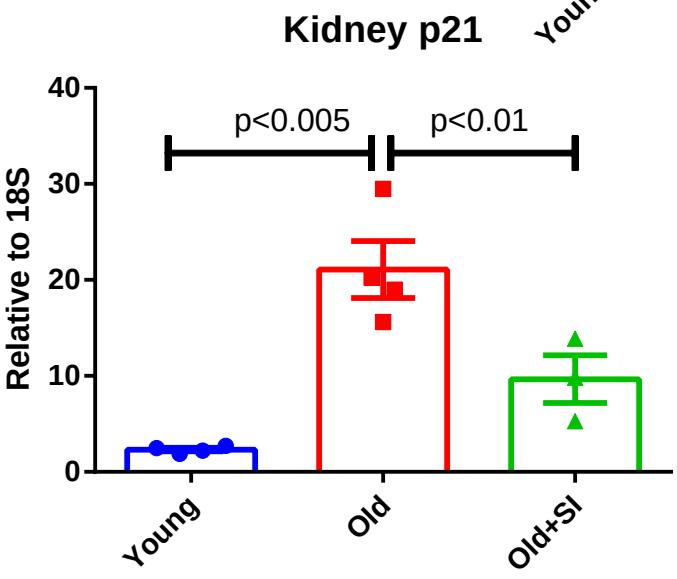
Kidney p21
p<0.005
p<0.01
Relative to 18S
40
30
20
10
0
Young
Old
Old+SI

Figure 7

B

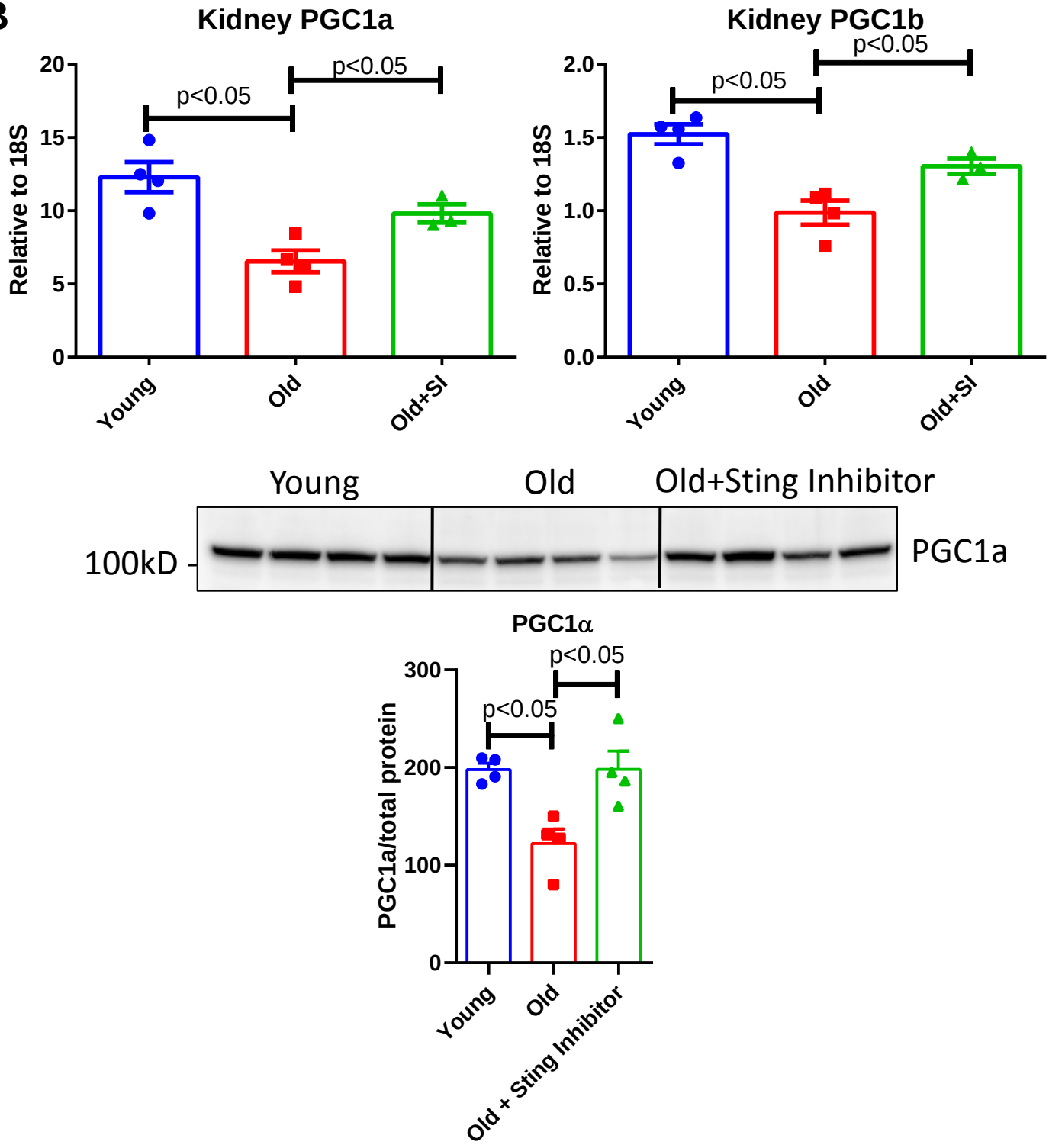
Kidney PGC1a
Relative to 18S
20
15
10
5
0
p<0.05
p<0.05
Young
Old
Old+SI
Kidney PGC1b
Relative to 18S
2.0
1.5
1.0
0.5
0.0
p<0.05
p<0.05
Young
Old
Old+SI
Young
Old
Old+Sting Inhibitor
100kD
PGC1a
PGC1α
PGC1a/total protein
300
200
100
0
p<0.05
p<0.05
Young
Old
Old + Sting Inhibitor

Figure 7

B

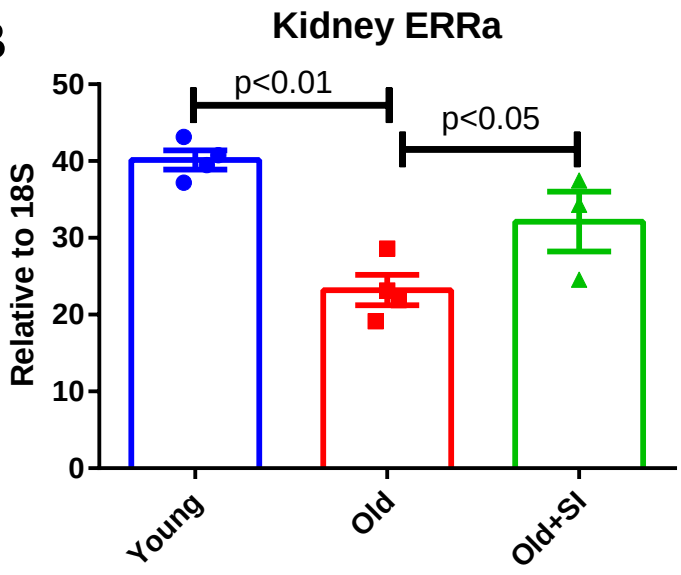
Kidney ERRa
Relative to 18S
50
40
30
20
10
0
p<0.01
p<0.05
Young
Old
Old+SI

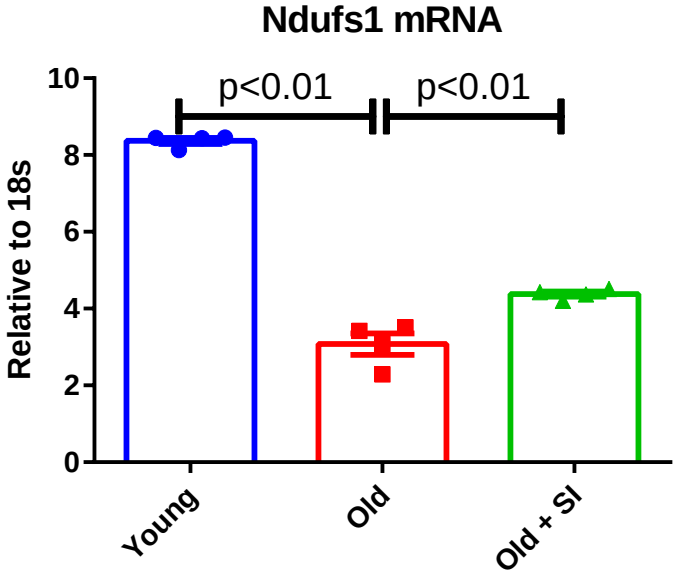
Ndufs1 mRNA
Relative to 18s
10
8
6
4
2
0
p<0.01
p<0.01
Young
Old
Old + SI

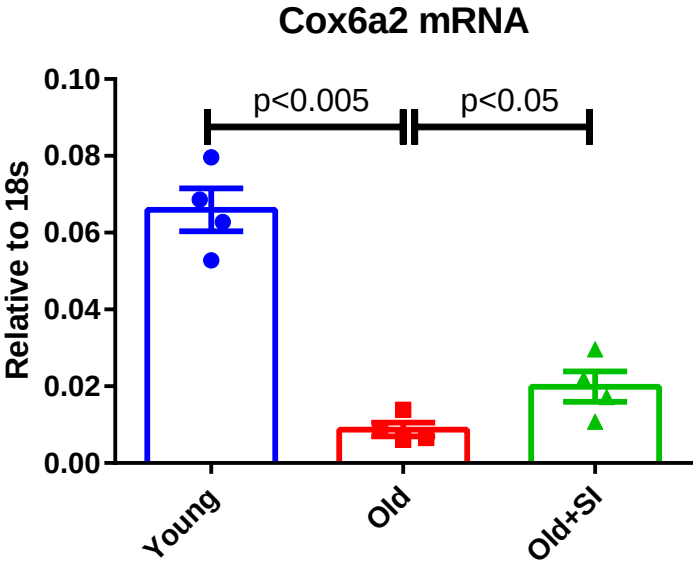
Cox6a2 mRNA
Relative to 18s
0.10
0.08
0.06
0.04
0.02
0.00
p<0.005
p<0.05
Young
Old
Old+SI

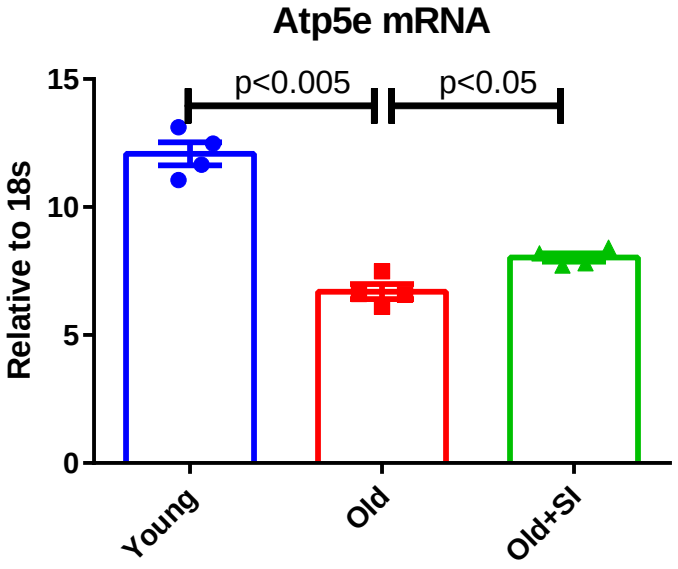
Atp5e mRNA
Relative to 18s
15
10
5
0
p<0.005
p<0.05
Young
Old
Old+SI

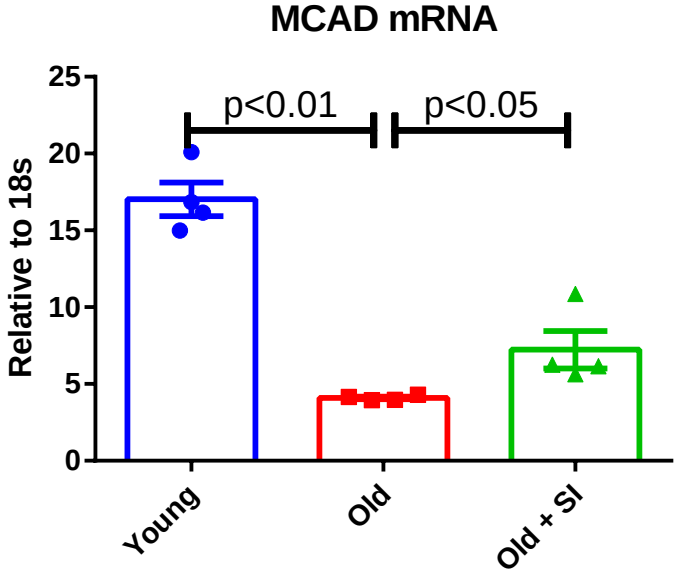
MCAD mRNA
Relative to 18s
25
20
15
10
5
0
p<0.01
p<0.05
Young
Old
Old + SI

Supplementary figure 1

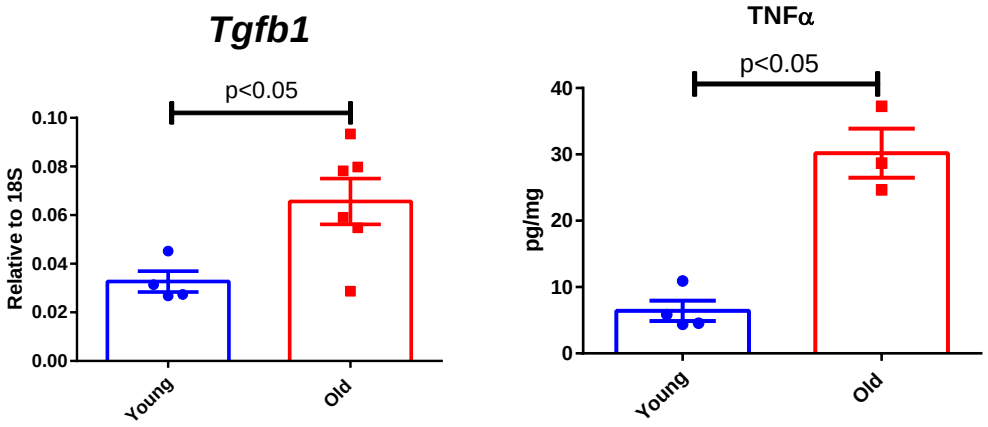

TGF-β mRNA and TNFα protein expression were increased in the aging kidney. n=4-6 samples per group.

Supplementary figure 2

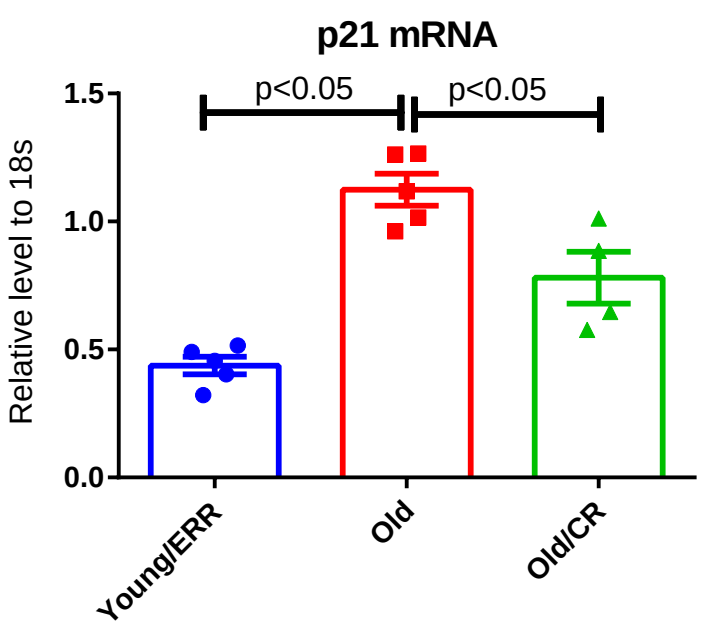

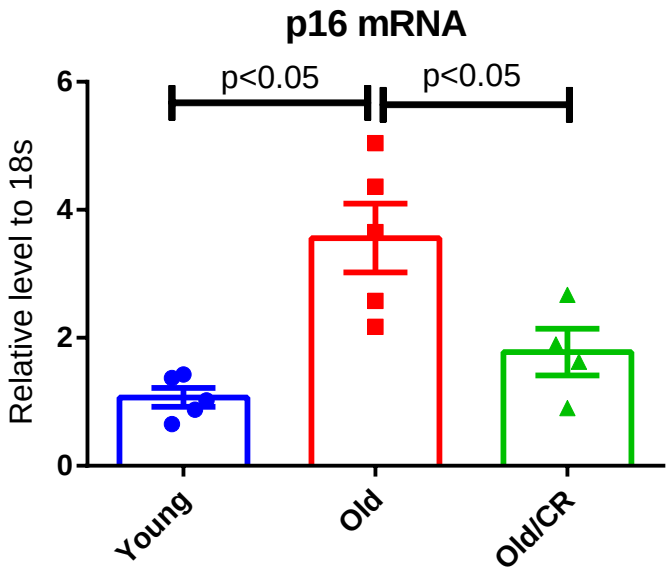

Cellular senescence markers p21 and p16 mRNA level was increased in the aging kidney. However in aging kidneys with life-long CR, p21 and p16 mRNA expression was downregulated compared to that in *ad lib* aging kidneys. n=4-5 samples per group.